THE HBP IN HYPERGLYCEMIA-ACCELERATED ATHEROSCLEROSIS

A METABOLIC APPROACH TO EXAMINING THE POTENTIAL ROLE OF THE HEXOSAMINE BIOSYNTHETIC PATHWAY IN DIABETES-ASSOCIATED ATHEROSCLEROSIS

By CHRISTINA I. PETLURA, B.Sc. (Hons.)

A Thesis Submitted to the School of Graduate Studies in Partial Fulfillment of the

Requirements for the Degree Master of Science

McMaster University MASTER OF SCIENCE (2014) Hamilton, Ontario (Chemical Biology)

TITLE: A Metabolic Approach to Examining the Potential Role of the Hexosamine Biosynthetic Pathway in Diabetes-Associated Atherosclerosis

AUTHOR: Christina I. Petlura, B.Sc. (McMaster University)

SUPERVISOR: Dr. Geoff Werstuck

NUMBER OF PAGES: xiii, 79

ABSTRACT

The number of people living with diabetes worldwide is continually increasing. The majority of these people will eventually die of cardiovascular disease, the major underlying cause of which is atherosclerosis. Despite the efforts of many researchers, gaps in our knowledge still exist regarding the molecular mechanism(s) linking the two conditions. Current data suggests that the hexosamine biosynthetic pathway (HBP) may have a role in the development of hyperglycemia-accelerated atherosclerosis. About 2-3% of glucose entering a cell is diverted into this pathway where it is modified through a series of reactions to yield the end product, UDP-*N*-acetylglucosamine (UDP-GlcNAc); a substrate for both *N*- and *O*-linked glycosylation of various molecules. *N*-linked glycosylation occurs in the endoplasmic reticulum (ER) and is an important process in the maintenance of ER homeostasis. We hypothesized that a dysregulation in the HBP can ultimately trigger ER stress – an event associated with the development of atherosclerosis. We have established a method that allows us to monitor levels of UDP-GlcNAc both in cultured cells and mouse tissues through high-performance liquid chromatography coupled to mass spectrometry (HPLC-MS). Using this technique, we've shown that both glucosamine supplementation and overexpression of the rate limiting enzyme of the HBP, GFAT, in cultured cells results in elevated UDP-GlcNAc levels. Furthermore, glucosamine was shown to trigger ER stress. In contrast, three GFAT inhibitors that were previously identified in a high throughput screen were shown to

decrease UDP-GlcNAc levels and one inhibitor, dehydroiso-β-lapachone, appears to prevent ER stress induction. Finally, we use complementary methods to show that the HBP is augmented in the livers of hyperglycemic mice. This process may play a role in the accelerated development of atherosclerosis. Together, these results provide further insight into the role of the HBP in diabetic atherosclerosis and the established methods provide a platform for the further investigation of this mechanism.

ACKNOWLEDGEMENTS

First and foremost, I would like to thank my supervisor, Dr. Geoff Werstuck, for all of his support, both personally and academically throughout the past two years. Your guidance and continual positivity motivated me to accomplish my goals and I am truly grateful for having had you as a mentor.

To my committee members, Drs. Fred Capretta and John Brennan, thank you for sharing your expertise with me and for all of your input throughout my project.

I'd like to thank Dr. Lisa Walter for providing me with a source of GFAT and allowing me to use her inhibitors, as well as for her assistance in the initial stages of my project. Thank you to Dr. Ken Chalcraft for taking the time to train me on the HPLC-MS system and for all of his advice and input into the development of the HPLC-MS method. To Vi Dang, thanks for your help with running the HPLC-MS samples initially, with all the troubleshooting, and for making me laugh.

Thank you to Elna Luckham and the Biointerfaces Institute for providing me with a facility and state-of-the-art equipment to perform my experiments on.

Thank you to all of the Werstuck lab members, past and present, for putting up with me and making my time at TaARI enjoyable. Special thanks to Dr. Peter Shi for harvesting mice for me, and Daniel Venegas-Pino for providing me with aortic sections. Also thank you to Mark Fuller for his assistance in tissue sectioning.

I'd like to thank Tammy Feher for all of her administrative assistance.

Lastly, I'd like to express my gratitude to all of my friends (especially AZ) and family for their continuous love and support during these last two years. Thank you for all of your encouragement, and for always being there. I owe much of my success to you.

TABLE OF CONTENTS

LIST OF TABLES

LIST OF FIGURES

ABBREVIATIONS

ACN	Acetonitrile
Ad	Adenovirus
AGE	Advanced glycation end-product
ANOVA	Analysis of variance
APCI	Atmospheric pressure chemical ionization
ApoB-100	Apolipoprotein B-100
ApoE	Apolipoprotein E
APPI	Atmospheric pressure photoionization
ATF6	Activating transcription factor 6
CMV	Cytomegalovirus
CVD	Cardiovascular disease
DAG	Diacylglycerol
DAPI	4',6-diamidino-2-phenylindole
DHAP	Dihydroxyacetone phosphate
DON	6-diazo-5-oxo-norleucine
DTT	Dithiothreitol
EC	Endothelial cell
EDTA	Ethylenediaminetetraacetic acid
eIF2α	Eukaryotic translation initiation factor 2 alpha
ER	Endoplasmic reticulum
ERAD	Endoplasmic reticulum -associated degradation
ESI	Electrospray ionization
F6P	Fructose-6-phosphate
FBG	Fasting blood glucose
G6P	Glucose-6-phosphate
GAPDH	Glyceraldehyde 3-phosphate dehydrogenase
GFAT	L-glutamine: D-fructose-6 phosphate amidotransferase
GFP	Green fluorescent protein
Glc	Glucose
GlcN	Glucosamine
GlcN6P	Glucosamine-6-phosphate
GlcNAc6P	*N*-acetyl glucosamine-6-phosphate
Gln	L- glutamine
Glu	L-glutamate
Gly-Phe	Glycine-phenylalanine
Grp78	Glucose regulatory protein 78
Grp94	Glucose regulatory protein 94
GSH	Glutathione

GSSG	Glutathione disulfide
H&E	Hematoxylin and eosin
HBP	Hexosamine biosynthetic pathway
HBSS	Hanks' balanced salt solution
HepG2	Human hepatocarcinoma
HILIC	Hydrophilic interaction liquid chromatography
HPLC	High performance liquid chromatography
IF	Immunofluorescence
Ins2	Insulin 2
IRE1	Inositol-requiring enzyme-1
IRES	Internal ribosomal entry sequence
IRS	Insulin receptor substrate
IS	Internal standard
ITO	Indium tin oxide
KDEL	Lysine, Glutamic acid, Aspartic acid, Leucine
LDL	Low density lipoprotein
LDLr	Low-density lipoprotein receptor
MALDI	Matrix-assisted laser desorption ionization
MALDI-IMS	MALDI imaging mass spectrometry
MeOH	Methanol
MI	Myocardial infarction
mOCT	Modified Optimal Cutting Temperature compound
MOI	Multiplicity of infection
M.O.M.	Mouse on mouse
MOVAS	Mouse vascular smooth muscle
MS	Mass spectrometry
m/z	Mass to charge
NAD^+	Nicotinamide adenine dinucleotide
Nd:YAG	Neodymium-doped yttrium aluminium garnet
O-GlcNAc	O-linked *N*-acetylglucosamine
PBS	Phosphate buffered saline
PERK	Protein kinase RNA-like endoplasmic reticulum kinase
PFK	Phosphofructokinase
PI	Phosphatidylinositol
PKC	Protein kinase C
PMA	Phorbol 12-myristate 13-acetate
PPG	Polypropylene glycol
PVA	Polyvinyl alcohol
Q-TOF	Quadrupole time-of-flight
RAGE	Receptor for advanced glycation end products

RCF	Relative centrifugal force
ROS	Reactive oxygen species
RRF	Relative response factor
SDS-PAGE	Sodium dodecyl sulphate polyacrylamide gel electrophoresis
SMC	Smooth muscle cell
STZ	Streptozotocin
T1D	Type 1 diabetes
T2D	Type 2 diabetes
TBST	Tris-Buffered Saline and Tween 20
TOF	Time-of-flight
UDP-GlcNAc	Uridine diphosphate *N*-acetylglucosamine
UPR	Unfolded protein response
UV/vis	Ultraviolet/visible
VLDL	Very low density lipoprotein
ZIC	Zwitterionic

CHAPTER 1. INTRODUCTION

1.1 Diabetes and its link to atherosclerosis

Diabetes mellitus is a disease characterized by hyperglycemia resulting from a deficiency in insulin function that affects millions of people worldwide and can lead to a variety of complications, including cardiovascular disease (CVD), nephropathy and retinopathy (*1*). The disease can be divided into two types: type 1 diabetes (T1D) – an autoimmune disorder in which the body's own cells destroy its pancreatic beta cells resulting in the production of very little or no insulin, and type 2 diabetes (T2D), which is characterized by insulin resistance caused by a defect in insulin signaling that reduces tissue sensitivity to the insulin released into the bloodstream (*2, 3*). CVD is the most common cause of mortality for people with either T1D or T2D, accounting for about 70% of deaths (*4*). The major underlying cause of CVD is atherosclerosis, which is an inflammatory disease of the large arteries. The development of an atherosclerotic lesion begins with damage to endothelial cells that line the innermost layer of the artery, the intima (**Figure 1**) (*5*). This initial insult to the endothelium can result from various factors, including hypertension, hypercholesterolemia or smoking. As a response to the damage, endothelial cells present adhesive molecules that mediate the infiltration of circulating monocytes and T cells, which accumulate in the intimal space (*6*). These monocytes then differentiate into macrophages that secrete cytokines that amplify the recruitment of monocytes. Macrophages endocytose low density lipoprotein (LDL) and

oxidized LDL particles that invade the arterial wall, resulting in the formation of lipid-engorged macrophage foam cells that create fatty streaks in the artery wall. These foam cells secrete cytokines, which induce the movement of vascular smooth muscle cells (SMCs) from the media layer of the artery into the intima (*6*). The SMCs synthesize collagen fibres that form a fibrous cap over the lesion. Foam cells eventually undergo apoptosis, creating an acellular, cholesterol-rich necrotic core that destabilizes the lesion (*7*). Thrombosis results when the lesion ruptures, allowing blood to come into contact with the lesion, which could lead to total occlusion of the artery and cause myocardial infarction (MI). The pathology of atherosclerosis appears to be independent of any risk factors associated with disease progression. Despite a vast amount of research, the molecular mechanisms that link diabetes to CVD are not well understood.

Four mechanisms have been proposed to explain how hyperglycemia promotes atherosclerosis: activation of protein kinase C (PKC) (*8*), increased production of advanced glycation end-products (AGEs) (*9*), and increased flux through the polyol and hexosamine biosynthetic pathways (*10*) (**Figure 2**). PKC triggers the activation of various pathways contributing to diabetic complications and is itself activated by diacylglycerol (DAG), a molecule produced from the glycolytic intermediate glyceraldehyde-3-phosphate, which accumulates in hyperglycemic conditions (*11*). AGEs are formed from the reaction of oxidized derivatives of certain glycolytic intermediates with proteins, initiated by high glucose levels (*9*). They contribute to CVD through binding to the AGE

receptor (RAGE) and activating transcription factors involved in inflammation and endothelial dysfunction (*12*). Excess glucose can also be diverted to the polyol pathway where it is reduced to sorbitol in an NADPH-dependent process by the enzyme aldose reductase (*10*). Sorbitol is then converted into fructose using the cofactor nicotinamide adenine dinucleotide (NAD$^+$) and producing NADH. The depletion of NADPH results in vascular consequences by decreasing the levels of reduced glutathione (GSH), which deteriorates the cell's ability to protect itself against reactive oxygen species (ROS) that cause vascular damage. Finally, excess glucose can enter the hexosamine biosynthetic pathway (HBP), leading to the overexpression of the rate limiting enzyme in the pathway glutamine:fructose-6 phosphate amidotransferase (GFAT). Overexpression of GFAT has been shown to disrupt the function of β-cells resulting in diabetic complications (*13*). Furthermore, treatment of β-cells with glucosamine, a precursor in the HBP, results in an increase in hydrogen peroxide levels suggesting that increased flux through the HBP deteriorates β-cell function by inducing oxidative stress.

Each of the above mechanisms is enhanced by oxidative stress. Hyperglycemia causes an increase in glycolytic flux leading to a higher production of mitochondrial ROS, which partially inhibit the glycolytic enzyme glyceraldehyde 3-phosphate dehydrogenase (GAPDH) thereby diverting the upstream metabolites into these pathways (**Figure 2**) (*10*). Despite the fact that antioxidants have been shown to effectively inhibit these pathways *in vitro (13-16)*, antioxidant therapies have shown no cardiovascular benefit in

virtually every well controlled clinical trial in which they were tested (*17-22*). This suggests that some other mechanism(s) may be contributing to diabetes-associated CVD.

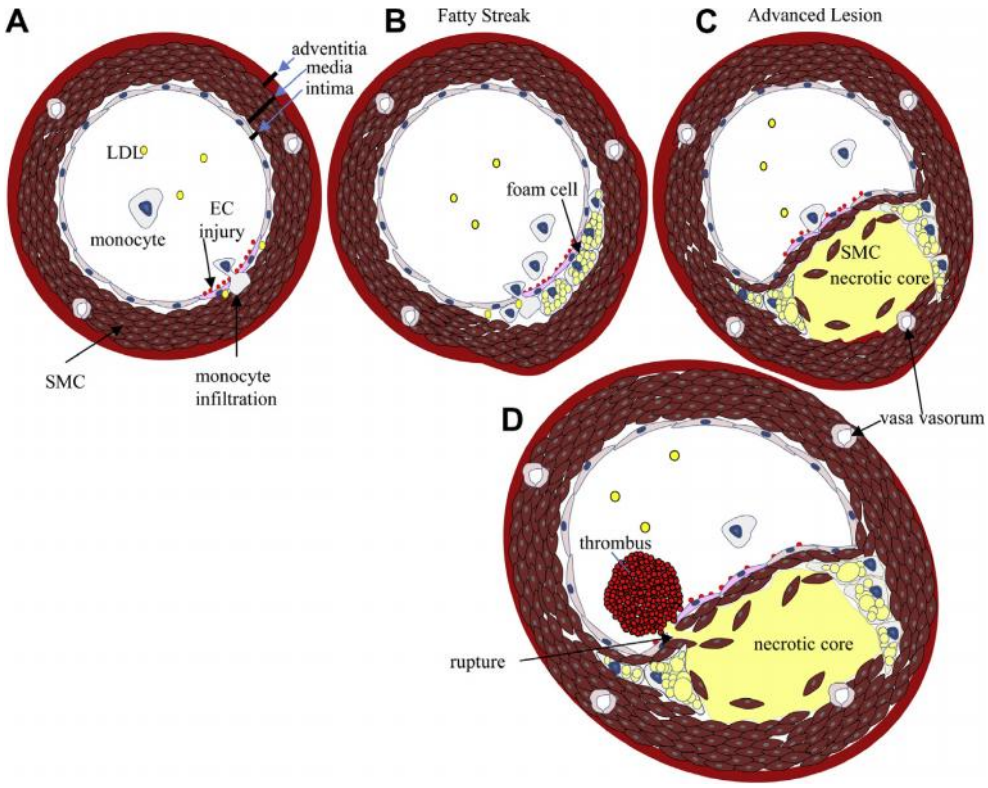

Figure 1 | The development of an atherosclerotic lesion. (A) An EC injury is the initial event in atherogenesis. Damaged endothelial cells present adhesive molecules, such as vascular cell adhesion molecule-1 and P-selectin, attracting circulating monocytes and T cells that accumulate at the site of injury. Some of these inflammatory cells move into the subendothelial intima. (B) Intimal monocytes differentiate into macrophages that secrete cytokines and exacerbate the inflammatory environment. Macrophages also endocytose LDL and oxidized LDL particles, becoming lipid-engorged foam cells. (C) Vascular SMCs migrate into the intima where they proliferate and secrete collagen fibres that form a fibrous cap over the lesion. Macrophage/foam cells undergo apoptosis, resulting in the formation of a cholesterol-rich necrotic core that destabilizes the lesion. (D) If the atherosclerotic lesion ruptures and blood contacts the contents of the lesion, a thrombus will form. This can lead to local occlusion of the artery and result in a myocardial infarction. EC, Endothelial cell; LDL, low-density lipoprotein; SMC, smooth muscle cell. Taken from Zeadin et al. (2013).

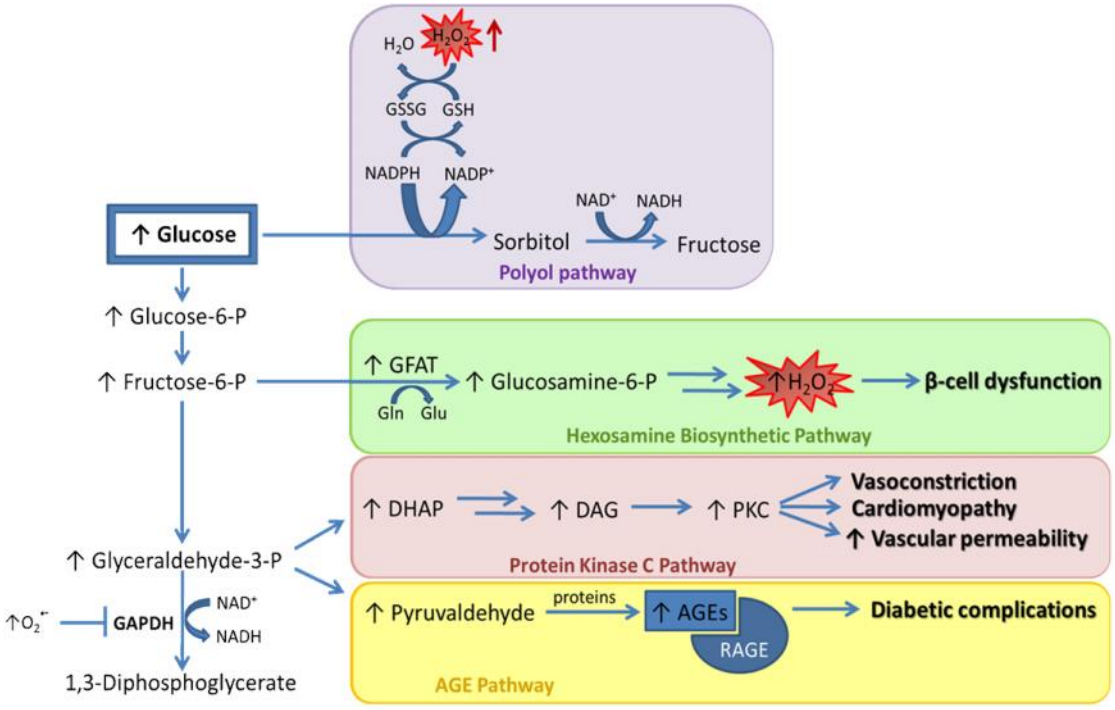

Figure 2 | Proposed mechanisms of hyperglycemia-induced atherosclerosis. Hyperglycemia causes an increase in glycolytic flux resulting in higher mitochondrial ROS production, such as the superoxide anion radial species. These ROS partially inhibit the glycolytic enzyme GAPDH, diverting upstream metabolites into non-oxidative glucose pathways which include the polyol, hexosamine biosynthetic, protein kinase C and AGE pathways. Activation of these pathways contributes to the vascular complications associated with hyperglycemia. GSSG: glutathione disulfide; GSH: glutathione; GFAT: glutamine:fructose-6 phosphate amidotransferase; Gln: glutamine; Glu: glutamate; DHAP: dihydroxyacetone phosphate; DAG: diacylglycerol; PKC: protein kinase C; AGEs: advanced glycation end-products; RAGE: AGE receptor; GAPDH: glyceraldehyde 3-phosphate dehydrogenase. Adapted from Brownlee, M. (2001).

1.2 The Hexosamine Biosynthetic Pathway

The accumulation of glucosamine, observed in models of hyperglycemia-induced atherosclerosis, suggests a role for the HBP in linking diabetes to atherosclerosis (*23, 24*). We hypothesize that the HBP is linked to another mechanism not associated with oxidative stress that could, in part, account for the cardiovascular phenotypic features found in diabetic individuals. The HBP begins with the formation of glucosamine-6-phosphate (GlcN-6-P) from fructose 6-phosphate (F6P) and glutamine (Gln) or directly

from glucosamine (GlcN), which enters the cell via the glucose transport system (*25, 26*) (**Figure 3**). F6P is produced from glucose entering the cell, 2-3% of which is diverted into the HBP rather than proceeding through glycolysis (*27*). One of the challenges in investigating the effects of hyperglycemia on the HBP in cell culture arises from the difficulty in increasing HBP flux with high glucose alone, since most of the glucose taken up by rapidly growing/dividing cultured cells is utilized for energy production through glycolysis rather than entering the HBP. Therefore, overexpression of GFAT alone would likely not cause a large increase in flux through this pathway as the turnover capacity is limited by the quantity of substrates available. Fructose-6 phosphate is a common metabolite of glycolysis and the HBP, thus in order to increase the amount of F6P going into the latter pathway, the enzyme responsible for its conversion in the glycolytic pathway can be inhibited (**Figure 3**). This enzyme is phosphofructokinase (PFK), which phosphorylates fructose-6 phosphate to fructose-1,6-bisphosphate (*28*). In normal cells, PFK is a highly regulated enzyme that is induced by insulin and allosterically activated by AMP in the presence of high glucose, and repressed by glucagon and allosterically inhibited by ATP and citrate during gluconeogenesis (*28, 29*). Citrate is produced in the citric acid cycle, and its accumulation, along with that of ATP, indicates a high cellular energy state, preventing the need for further glucose metabolism (*28*).

Hyperglycemia increases flux through the HBP as more glucose is available for the conversion to F6P. The formation of GlcN-6-P is the rate limiting step in this pathway

and the enzyme responsible for its production is glutamine:fructose-6 phosphate amidotransferase (GFAT) (*30*). GlcN-6-P is then acetylated by the enzyme glucosamine-6 phosphate *N*-acetyltransferase to produce *N*-acetyl glucosamine-6 phosphate (GlcNAc-6P), and this product is isomerized by phosphoacetylglucosamine mutase to give GlcNAc-1P (*31*). The final step is performed by UDP-N-acetylglucosamine pyrophosphorylase, which uses uridine triphosphate to produce uridine diphosphate N-acetylglucosamine (UDP-GlcNAc), the end product of the pathway. UDP-GlcNAc is a metabolite of interest because it is a substrate for *N*- and *O*-linked glycosylation of various proteins and lipids (*32*). UDP-GlcNAc is O-linked to serine and threonine residues on proteins by the enzyme *O*-GlcNAc transferase (OGT) (*33*). Proteins regulated by O-GlcNAcylation include the insulin receptor substrates (IRS)-1 and -2 (*32*), raising the possibility that a dysregulation in the HBP may affect the function of these proteins and cause insulin resistance.

N-linked glycosylation occurs on newly synthesized proteins in the endoplasmic reticulum (ER). This process requires UDP-GlcNAc for the synthesis of the donor dolichylpyrophosphate that is used in the assemble of a complex lipid linked oligosaccharide that ultimately is attached to an asparagine residue on the nascent protein (*34*).

Overproduction of UDP-GlcNAc has been implicated in the activation of a transcription factor that induces the expression of plasminogen activator inhibitor-1, a

protein that inhibits the breakdown of blood clots (*11, 32*). In addition, research has shown that an increase in flux through the HBP due to hyperglycemia, or with the addition of exogenous glucosamine, can disrupt protein folding in the ER, triggering ER stress (*23, 35-37*) (**Figure 4**). Our lab and others have demonstrated that ER stress can stimulate lipid biosynthesis, inflammatory factor expression and endothelial cell/macrophage apoptosis – events associated with atherogenesis (*35, 38, 39*).

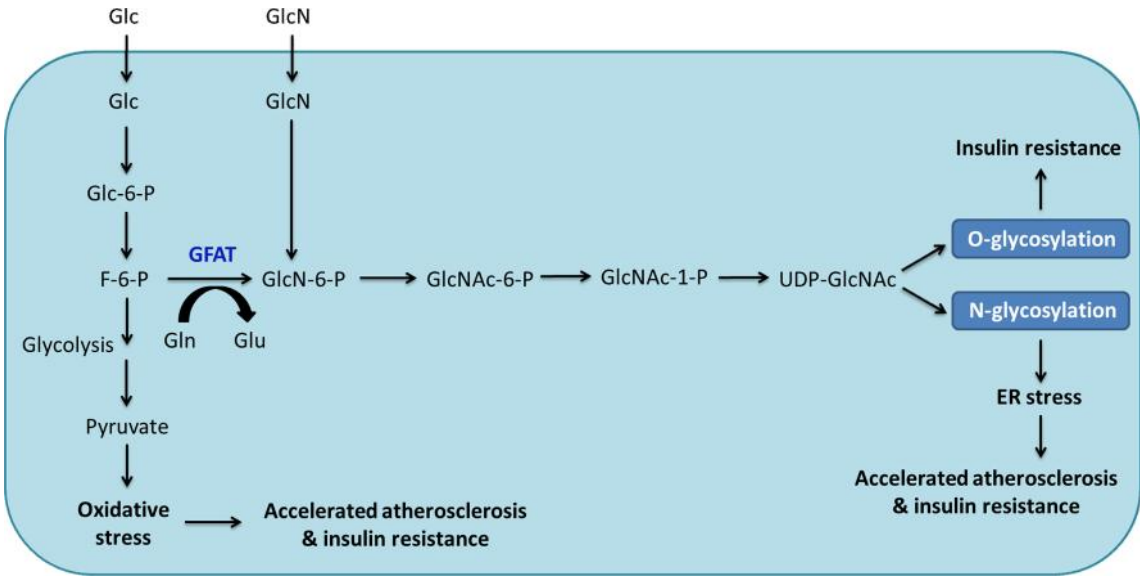

Figure 3 | The hexosamine biosynthetic pathway and its role in diabetic complications. The pathway begins with the formation of glucosamine-6 phosphate (GlcN-6-P) either from fructose-6 phosphate (F-6-P) and glutamine (Gln) or from glucosamine (GlcN) entering the cell. The final product, UDP-GlcNAc, is used for the glycosylation of various proteins and lipids. Both the glycolytic and the hexosamine biosynthetic pathways have been implicated in hyperglycemia-induced diabetic complications through largely unknown mechanisms. A dysregulation in *N*-linked glycosylation may disrupt protein folding in the ER, triggering ER stress, which has been associated with accelerated atherosclerosis and insulin resistance. Glc: glucose; Glu: glutamate.

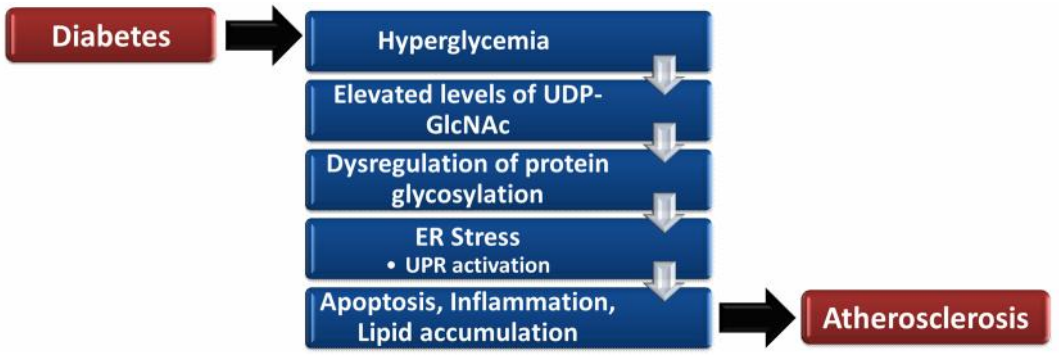

Figure 4 | Our hypothesis linking diabetes to atherosclerosis. Series of events we hypothesize may link diabetes to atherosclerosis by increased flux through the hexosamine biosynthetic pathway and the induction of ER stress.

1.3 ER stress and the unfolded protein response (UPR)

The ER is a cell organelle involved in the synthesis and transport of proteins. Integrated quality control mechanisms ensure that only properly folded, and thus functional, proteins are secreted (*40*). Specific protein modifications assist in correct folding and include the formation of disulfide bonds or glycosylation of an asparagine or arginine residue (*41, 42*). The folding process is accomplished with the help of chaperone proteins located in the ER, including Grp78, Grp94 and calreticulin as well as foldases, such as protein disulfide isomerase (*40*). A variety of stimuli, including hypercholesterolemia, obesity and hypertension, have been associated with the induction of ER stress and activation of the unfolded protein response (UPR) (**Figure 5**) (*43*). The UPR functions to regain homeostasis by inhibiting *de novo* protein synthesis, increasing the folding capacity of the ER though the overexpression of ER chaperones and degrading terminally misfolded proteins (*36*). During ER stress, the ER chaperone Grp78 dissociates from three ER membrane-bound proteins, PERK, ATF6 and IRE1,

leading to their activation (*43*). Activation of PERK leads to inhibition of eIF2α, an initiation factor required for mRNA translation, thus decreasing *de novo* protein synthesis. Activation of IRE1 and ATF6 mediate the overexpression of ER chaperones and ER-associated degradation (ERAD) proteins. These responses attenuate ER stress thereby restoring ER homeostasis. Many of the ER chaperone proteins, including Grp78 and Grp94, contain a characteristic sequence of four amino acids at their carboxy terminal – lysine-aspartic acid-glutamic acid-leucine (KDEL) (*44*)– that acts as an anchor sequence to retain them in the ER. KDEL is used by researchers as a marker for the identification and quantification of ER resident proteins.

The fact that the accumulation of misfolded proteins induces ER stress, and that UDP-GlcNAc is a major substrate for protein modification suggests that a dysregulation in the HBP may contribute to the development of ER stress. Furthermore, increased GFAT and O-GlcNAcylation levels have been observed in a mouse model of hyperglycemia-induced atherosclerosis, making this enzyme a potential target for therapeutic intervention (*45*).

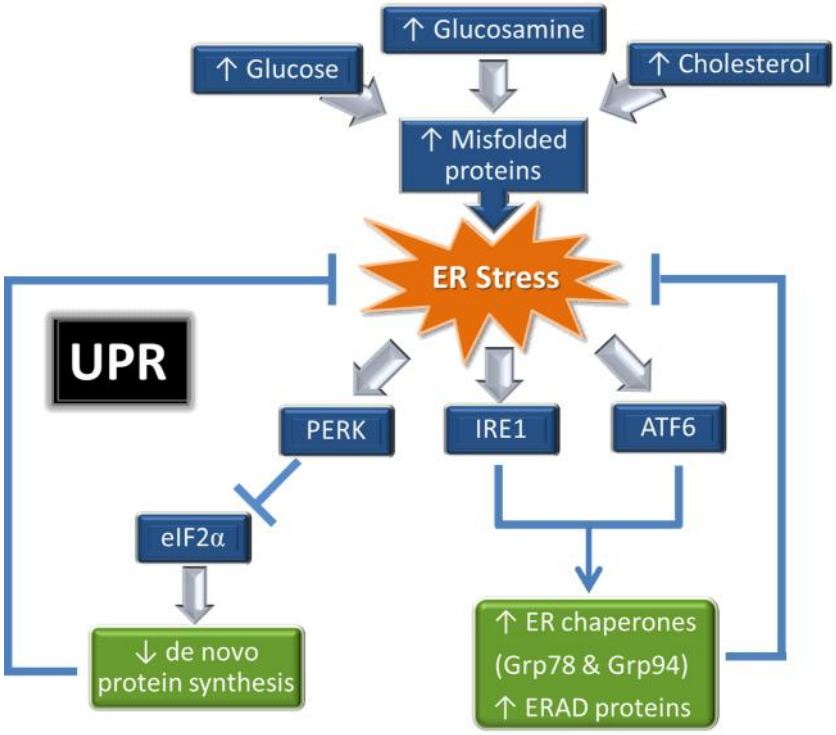

Figure 5 | Factors contributing to the activation of the unfolded protein response (UPR) and its mechanism of restoring ER homeostasis. The accumulation of misfolded proteins from various stimuli results in the induction of ER stress. The cellular response to ER stress is the activation of membrane-bound ER-associated proteins PERK, IRE1 and ATF6, which function to attenuate ER stress. Activation of PERK leads to inhibition of eIF2α, an initiation factor required for mRNA translation, thus decreasing *de novo* protein synthesis. IRE1 and ATF6 mediate the overexpression of ER chaperones (Grp78 and Grp94) and ER-associated degradation (ERAD) proteins. These responses attenuate ER stress thereby restoring ER homestasis.

1.4 GFAT function and activity assays

GFAT is an enzyme composed of an N-terminal glutaminase domain, the site of glutamine binding, and a C-terminal isomerase domain for F6P binding (*46*). F6P binds to GFAT before glutamine and the binding affinity of F6P is greater than that of glutamine (K_m = 0.2-1 mM compared to K_m = 0.4-2 mM) (*47*). Biologically, the bacterial form of the enzyme exists as a dimer while the eukaryotic version has a tetrameric structure in solution (*48*). The most characterized form of the enzyme is that from *E. coli*, which is

known to exhibit three other catalytic activities in addition to the synthase activity. It can produce glutamate from glutamine either in the presence of both substrates through its hemisynthase activity, or in the absence of F6P by its glutaminase activity (*48*). Additionally, in the absence of glutamine, it functions as an isomerase, converting F6P into glucose-6 phosphate (G6P) (*49*).

The eukaryotic form of GFAT is regulated through feedback inhibition by UDP-GlcNAc (*47*). To date only a handful of small molecule GFAT inhibitors have been discovered, including the glutamine analogues azaserine (*50*) and 6-diazo-5-oxo-norleucine (DON) (*27*). These compounds form a covalent bond with the enzyme in the glutamine binding pocket, making them irreversible inhibitors (*27*). Although these molecules provide insight into the role of GFAT in regulating HBP flux, they are not suitable candidates for drug development for the prevention of hyperglycemia-induced atherosclerosis because of their lack of specificity and their general cytotoxicity. The Capretta/Werstuck labs have recently identified several novel small molecule GFAT inhibitors *in vitro* using high throughput screening methods, including a new class of compounds containing the naphthoquinone core (*51*). These compounds were identified with the use of the Morgan-Elson assay, which detects N-acetylglucosamine (*52*). The assay works on the basis of detecting the amount of GlcN-6-P produced from its two substrates in the presence of GFAT. The GlcN-6-P produced is acetylated with 1.5% acetic anhydride and potassium tetraborate. The acetylated product is then reacted with

Ehrlich's reagent, which changes in colour from yellow to purple in the presence of product. The absorbance measured at 585 nm allows for the quantification and comparison of GlcN-6-P levels between treatments and controls and for the identification of GFAT inhibitors. Two major limitations of this assay are its poor sensitivity and its incompatibility for use with coloured compounds, as they interfere with and alter the absorbance measurement.

Recently, a novel technique for monitoring GFAT activity was established using matrix-assisted laser desorption ionization time-of-flight mass spectrometry (MALDI-TOF-MS) that overcomes the aforementioned limitations (*53*). This assay is capable of monitoring the production of GlcN-6-P and L-glutamate simultaneously, which allows for the screening of inhibitors that block both the F6P and glutamine binding sites. The assay is performed in a 96-well plate format, incubating the substrates with GFAT for 20 min at 37°C followed by terminating the reaction by heating at 99°C for 4 min. After centrifugation, the contents are transferred to microtubes and the products are *N*-acetylated in order to distinguish with formed GlcN-6-P from the excess F6P added. Once prepared, the samples are mixed with the matrix solution and spotted onto a slide for data acquisition.

1.5 High performance liquid chromatography-mass spectrometry

The compounds identified as inhibitors of GFAT *in vitro* can be further characterized in cultured cells using high performance liquid chromatography coupled to

mass spectrometry (HPLC-MS). This technique works on the basis of first separating compounds of different physical properties through a column followed by detecting them according to their mass to charge ratio.

HPLC is a method widely used in biochemistry for the separation and identification of various compounds in biological matrices (*54*). These matrices include cell lysates, biological fluids and whole tissue samples that must be carefully processed prior to their analysis by HPLC. Sample preparation is a crucial step in the analysis process as the sample is processed with the purpose of making it compatible for HPLC, eliminating interferences and retaining the metabolite(s) of interest (*54*). This involves the selection of suitable solvents and extraction methods and varies depending on the matrix and metabolites chosen. A common procedure used for the removal of lipids from tissue samples is the Folch method (*55*). This procedure involves homogenization of the tissue in a 2:1 chloroform:methanol mixture followed by the addition of 20% of the tissue extract's volume of water. Subsequent filtration and centrifugation forms two distinct layers; the upper methanol layer contains the polar compounds such as carbohydrates while the lower chloroform layer is composed of non-polar compounds, including lipids. This method is also useful for the removal of non-soluble proteins, which precipitate during the extraction process.

Once the sample is prepared, its components are separated through a column, allowing for identification or quantification of individual species. The choice of column is

dependent on the physical properties of the analyte(s); charged compounds can be separated on ionic exchange columns, non-polar compounds are retained on reversed phase (hydrophobic) columns while polar compounds require a normal (hydrophilic) stationary phase. The hydrophilic interaction liquid chromatography (HILIC) mode is often used for carbohydrate separation through various silica-based stationary phases containing polar functional groups including diol, amine, amide and zwitterionic (ZIC-HILIC) groups (*56*-*58*). The analytes reach an equilibrium between the mobile and stationary phases and elute with a specific retention time based on the strength of their interactions with each phase. The mobile phase composition is either kept constant throughout the separation or varied, resulting in a gradient elution (*59*). For the separation of carbohydrates using a normal phase column, a gradient elution of increasing solvent polarity gives the compounds time to achieve equilibrium with the phases, yet elute with a shorter retention time, preventing peak broadening.

Following separation by HPLC, the compounds are detected either by ultraviolet/visible (UV/vis) or mass spectrometry. UV/vis detection requires the presence of a chromophore in the molecule(s) of interest capable of absorbing light in the ultraviolet or visible regions of the absorption spectrum or chemical derivatization of the molecule with a chromophore (*60*). Alternatively, detection by mass spectrometry is based on the ionization efficiency of the compound(s) and requires only a minute amount of sample due to its supreme sensitivity (*60*). Common ionization techniques

include electrospray ionization (ESI), atmospheric pressure chemical or photoionization (APCI and APPI), and matrix-assisted laser desorption ionization (MALDI) (*61*). ESI is a soft ionization method that leaves the parent ions intact, making it useful in the analysis of biological compounds as their exact structure in the original sample can be determined. APCI and APPI generate more fragment ions compared to ESI and operate at high flow-rates and temperatures, limiting their use to the analysis of small, thermally stable molecules (*60*). MALDI is another soft ionization technique commonly used in the analysis of fragile biomolecules such as peptides or DNA. Following HPLC separation, the analyte(s) are mixed with a matrix solution and spotted onto a MALDI plate (*62*); the matrix absorbs laser energy causing desorption and ionization of its upper layer and subsequent proton transfer to the analyte(s) (*63*). There have been rapid technological improvements in the past decade in MS techniques, including the emergence of MALDI imaging mass spectrometry (MALDI-IMS). This technique combines the sensitivity of mass spectrometry with imaging, permitting the study of the localization of numerous biomolecules simultaneously (*64*). MALDI-IMS was recently used to investigate markers of aortic atherosclerotic lesions in mice and humans, revealing the presence of lipid-rich and calcified regions in the lesions, which correlated to images obtained by H&E and immunostaining (*65*). This technique has also been used for the localization analysis of several primary metabolites, including UDP-GlcNAc, in brain tissue sections of rats in which 9-aminoacridine was identified as a powerful matrix for these analytes (*66*).

The final component of a mass spectrometer is the mass analyzer, in which the formed ions are separated based on their mass to charge (m/z) ratios. Examples of mass analyzers include time-of-flight (TOF), ion traps or quadrupoles (Q) (*60*). The analyzers can also be used in tandem (eg. Q-TOF) to provide additional information on the analyte(s) such as fragmentation patterns, which assist in structure determination (*61*). The quadrupole mass analyzer functions by generating electric fields between two sets of parallel rods through which ions are accelerated (*60*). An alternating voltage is applied to the rods, which allows only ions within a particular m/z range to pass and be detected. The ion trap analyzer works similarly but the ions are confined to an area by applying an electric field that stabilizes them, after which the desired analytes of specific m/z values are ejected by adjusting the field strength (*60*). The TOF analyzer functions by applying an external electric field, resulting in ions of the same charge possessing identical kinetic energies (*67*). The mass to charge ratio is determined by the time taken for the ions to reach the detector, as lighter ions will have faster velocities. This type of mass analyzer is useful for the identification of multiple compounds of different m/z values as all the ions can be simultaneously transmitted and detected. This approach allows for both targeted analyses, in which specific molecule(s) for analysis are pre-selected, and non-targeted analyses, in which the identities of molecule(s) varying between different treatments are determined after their detection, to be performed and can also be used for the study of metabolomics (*68*).

1.6 Mouse models of hyperglycemia-accelerated atherosclerosis

In order to obtain physiologically relevant data regarding the role of the hexosamine biosynthetic pathway in accelerating atherosclerosis, mouse models of hyperglycemia-accelerated atherosclerosis are used. Two methods used to chemically induce type 1 diabetes in mice are through alloxan or streptozotocin (STZ) injections, with the latter being the more commonly used method (*69, 70*). Both of these chemicals are toxic glucose analogues that are recognized by the GLUT2 glucose transporter due to their structural similarity to glucose (*69*). They selectively accumulate in pancreatic beta cells and cause cell death through different mechanisms; alloxan generates reactive oxygen species via the autoxidation of its reduction product, and the methylnitrosourea moiety of STZ acts as a DNA alkylating agent thereby destroying beta cells. Although inducing chemical diabetes is a fairly simple procedure, this process has several disadvantages, such as causing weight loss, stimulating glycemic shifts resulting in hypoglycaemia and causing respiratory distress (*71*).

Another means to induce diabetes is through genetic modification, an example of which is the $Ins2^{Akita}$ model (*72*). These mice possess one defective copy of the Ins2 gene, in which a point mutation (C96Y) prevents proper folding of the insulin protein. As a result, these mice produce very little functional insulin and develop hyperglycemia at about 4 weeks of age. The effects of this mutation are more severe in male than in female mice. This model overcomes the limitations of the chemically induced diabetes

models as the mice gain weight, although not as fast as normal, and they do not need to endure life-threatening glycemic shifts.

To permit the study of hyperglycemia-accelerated atherosclerosis, these hyperglycemic models must be used in conjunction with an atherosclerotic model. Two widely used models of atherosclerosis are the apolipoprotein E knockout ($ApoE^{-/-}$) and low-density lipoprotein (LDL) receptor deficient ($LDLr^{-/-}$) mice (*73*). ApoE is found on the surface of lipoproteins and is recognized by LDL receptors, resulting in the uptake of lipoproteins. The loss of ApoE thus prevents the clearance of lipoproteins causing an accumulation of lipids and the development of atherosclerosis even when these mice are fed a low-fat diet (*74*). LDLr is required for the uptake of LDL and VLDL via ApoB-100 and ApoE, respectively, thus loss of this receptor also leads to the accumulation of lipids and atherosclerosis development, but only when these mice are placed on a high-fat diet (*73*).

By combining the hyperglycemic $Ins2^{Akita}$ mice with the atherosclerotic $ApoE^{-/-}$ mice, a hyperglycemia-accelerated atherosclerosis model is created (**Figure 6**). This model does not require injections to induce diabetes nor a high-fat diet to develop atherosclerosis and is therefore the model of choice for examining the role of the hexosamine biosynthetic pathway in diabetes-induced atherosclerosis.

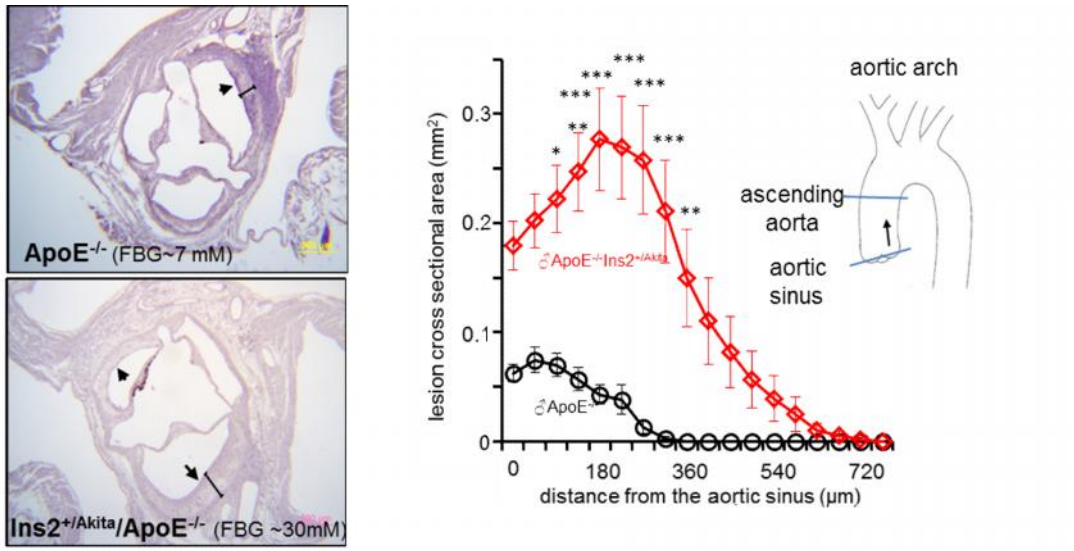

Figure 6 | Comparison of aortic lesion sizes in male ApoE$^{-/-}$ (black) and ApoE$^{-/-}$Ins2$^{+/Akita}$ (red) mice. All mice were analyzed at 25 weeks of age. FBG = fasting blood glucose. n=12 *P<0.5, **P<0.01, ***P<0.001 Venegas-Pino, D. et al (unpublished results).

CHAPTER 2. HYPOTHESES AND OBJECTIVES

The overall objective of this project is to gain a deeper understanding of the molecular mechanisms underlying the link between diabetes and hyperglycemia to the development of atherosclerosis. The main hypothesis for this project is that hyperglycemia results in increased flux through the HBP, which disrupts protein glycosylation. This event triggers ER stress, which ultimately contributes to the development of atherosclerosis. Manipulating the HBP by inhibiting GFAT should prevent the accumulation of glycosylated proteins and thus the onset of ER stress.

The **Specific Objectives** of this project are:

1. To establish the HPLC-MS system for monitoring HBP metabolites in both cultured cells and tissue samples and to use this system to assess the metabolic effects of manipulating the HBP by stimulating or inhibiting GFAT
2. To correlate the results obtained from our HPLC-MS studies to ER stress by examining the expression levels of ER stress markers in response to various treatments
3. To use MALDI imaging mass spectrometry and immunofluorescence staining techniques to compare levels of HBP metabolites in tissue samples of hyperglycemic mice to those of normoglycemic mice, and to relate these results to histological analyses of consecutive tissue sections thereby linking hyperglycemia to features associated with atherosclerosis.

CHAPTER 3. MATERIALS AND METHODS

3.1 Cell culture and treatment

Human hepatocarcinoma cells (HepG2) (ATCC) and Rat L6 skeletal muscle cells (ATCC® CRL-1458) were cultured in Dulbecco's modified Eagle's medium (DMEM) (Life Technologies, Burlington, Ontario) containing 10% fetal bovine serum, 1% Penicillin Streptomycin and either 5 mM (low) or 24.5 mM (high) glucose. Primary vascular aortic smooth muscle cells (MOVAS) (ATCC) were cultured in low glucose Dulbecco's modified Eagle's medium (DMEM) containing 10% fetal bovine serum and geneticin. Human monocytes (THP-1) (ATCC) were cultured in RPMI-1640 medium (Life Technologies) supplemented with 1% L-glutamine, 1% Hepes and 10% fetal bovine serum. THP-1 cells were differentiated into macrophages prior to treatment by the addition of phorbol 12-myristate 13-acetate (PMA) at 100 nM. The cells were left to differentiate for a minimum of 3 days. All cells were maintained at 37°C with 5% CO_2. HepG2 cells were treated with glucose (EM Science), glucosamine, amrinone, lapachol, alloxan, and dehydroiso-β-lapachone, all purchased from Sigma-Aldrich. Glucose and glucosamine (GlcN) were prepared directly in the medium while the GFAT inhibitors were dissolved in DMSO prior to dilution in the medium. To overexpress GFAT, cells were infected with an adenovirus vector (Ad-GFP-GFAT) 24 h following plating at an MOI of 25. After 60 min, the cells were rinsed with PBS. All cells were then cultured for an additional 48 h in high glucose DMEM. Infection efficiencies were determined by visualizing GFP expression. For

the citrate experiments, cells were treated with 1.75 mM ATP (Sigma-Aldrich) and either 1.25 or 2.5 mM tri-sodium citrate dihydrate (EMD Millipore) for various periods of time before harvesting.

3.2 HPLC-MS studies

3.2.1 Cell preparation

HepG2 cells were cultured in 12-well plates in DMEM until fully confluent. For the carbohydrate regulation studies, cells were cultured in low glucose medium for 48 hours followed by the addition of glucosamine (0.2-5 mM) or glucose (5-30 mM) for 24 hours. For *in vivo* inhibition studies, cells were cultured in high glucose medium and two hours prior to harvesting a GFAT inhibitor was added at 3 different concentrations (10, 20 and 50 µM). Each treatment was added to five wells and five additional wells were used as the positive control. For the GFAT overexpression study, cells were infected with Ad-GFP-GFAT or Ad-GFP (control) at an MOI of 25, for 24 hrs. Upon harvesting, the medium was removed and the cells were washed with 1x PBS buffer, pH 7.4. 300 µl of trypsin was added to each well and the plate was incubated at 37°C for 3 min. The cell solutions were transferred to eppendorf tubes and were centrifuged for 3 min at 13000 rpm at 4°C. The trypsin was aspirated and the pellets were resuspended in 100 µl of 1x PBS. Equal amounts of cell solution and Trypan Blue Stain 0.4% (Invitrogen) were mixed together for cell counting on the Countess® Automated Cell Counter. Each sample was counted in duplicate. The remainder of the cells were centrifuged for 10 min at 13000

rpm at 4°C and the supernatant was aspirated. The cells were resuspended in 100 µl of HPLC grade methanol (or 4:1 MeOH:H_2O) containing 20 µM of the internal standard Gly-Phe (Sigma-Aldrich). A small metal bead was added to each sample and the tubes were vortexed at maximum speed for 5 min. The beads were removed and the tubes were centrifuged for 15 min at 13000 rpm at 4°C. The supernatant was removed and used for HPLC analysis. The samples were stored at -20°C until analysis.

3.2.2 Tissue sample preparation

For the glucose tolerance experiment performed using human blood, 10 mL of blood was collected at each time point. An initial blood sample was taken in the fasting state. The subject then ingested a glucose drink containing 75 g of glucose and blood was taken after 2 and 4 hours. The blood samples were kept on ice for 1 hour, and were then inverted 10 times before being centrifuged at 1600 RCF for 20 min at room temperature. The upper plasma layer was discarded and the next layer containing mononuclear cells was transferred to a 15 mL conical tube. PBS was added to the sample up to a volume of 12 mL and the tube was spun for 15 min at 300 RCF. The supernatant was aspirated and the remaining cells were washed with 10 mL PBS then spun for 10 min at 300 RCF. The supernatant was discarded and the cell pellet was resuspended in 100 µL of 70:30 ACN:H_2O. The sample was passed through a 20 µm Millex-LG filter unit and stored at -20°C until analysis.

For the preparation of liver samples, frozen tissues from control ($ApoE^{-/-}$), hyperglycemic ($ApoE^{-/-}Ins2^{+/Akita}$) or glucosamine-treated ($ApoE^{-/-}$ with 5% GlcN in drinking water) male mice (25 weeks) were weighed out and placed into 15 mL conical tubes kept on ice. 3 mL of a 2:1 chloroform:methanol mixture with 7 µM internal standard (Gly-Phe) was added to each sample and they were homogenized. The samples were then agitated on a shaker for 20 min at room temperature followed by centrifugation at 2000 rpm for 3 min. The liquid phase was split among two 2 mL tubes and 20% of the sample volume of HPLC-grade water was added to each tube. Following vortexing, the samples were centrifuged at 2000 rpm for 20 min at 4°C. The upper layer was kept and dried down under a stream of N_2. The dried samples were resuspended in 100 µL of 70:30 ACN:H_2O then passed through Millex-LG filter units and diluted 20x prior to HPLC-MS analysis.

3.2.3 Analysis

Analysis of cell lysates was performed on an Agilent 1290 HPLC system connected to a Bruker ESI-MicroTOF. Samples (2 µl) were injected using the autosampler and sugars were separated by HPLC using the ZIC-cHILIC column (50 mm x 2.1 mm, 3 µm, 100 Å Merck® SeQuant) and detected by mass spectrometry on the Bruker ESI-MicroTOF. The mobile phase consisted of acetonitrile (A) and 10 mM ammonium acetate (B) (Caledon Laboratories Ltd). The flow rate was set to 0.2 mL/min and a binary solvent gradient was used (95 to 30% eluent A) over 20 min, followed by 15 min of equilibration.

The internal standard (20 µM Gly-Phe) and a pooled sample containing a portion of all the samples in the analysis was run after every five samples to ensure instrument functionality. The data was analyzed using the Bruker Daltonics DataAnalysis software. The relative response factor (RRF) was obtained by dividing the peak areas of UDP-GlcNAc (m/z 606.1) by the Gly-Phe internal standard (m/z 221.1). The values were normalized to the cell concentration determined in the sample preparation. The one-way ANOVA was employed for all statistical analyses, which were done using SigmaPlot software.

Tissue sample analysis was performed on a Thermo Ultimate 3000 HPLC system connected to a Bruker maXis 4G mass spectrometer. The method was similar to that above, except that the gradient elution was completed in 14 min followed by 10 min holding at 30% acetonitrile, and equilibration until 35 min. The peak areas of UDP-GlcNAc were normalized to that of the internal standard and tissue weight, where appropriate.

3.3 Immunoblot analysis

Cells were cultured in 6-well plates in low or high glucose DMEM for 48-72 h. Upon harvesting, the medium was removed and the cells were washed with cold PBS followed by the addition of 150 µl of lysis buffer (2% SDS, glycerol, 65 mM Tris-HCl pH 6.8). After 10 min, the cells were scraped off the plate and centrifuged for 10 min at 13000 rpm. The pellet was discarded and the protein concentration of each sample was determined

using the DC protein assay. Equal amounts of protein lysates were resolved by SDS-PAGE for 45 min at 195 V. The proteins were then transferred to nitrocellulose membranes, with the apparatus set at 200 mA for 90 min. Following transfer, the membranes were blocked in a 5% milk solution made up in TBST (50 mM Tris pH 7.4, 150 mM NaCl, 0.05% Tween-20) for 1 h, shaking. The 5% milk solution was replaced with a 1% milk solution to which KDEL (Lys-Asp-Glu-Leu, 1:1000), rabbit polyclonal GFAT (1:500; Santa Cruz Biotechnology), or RL2 (1:1000, Affinity Bioreagents Inc.) antibody was added. The blots were covered with Saran wrap and left gently shaking at 4°C overnight. The solution was removed and the blots were washed three times for 15 min with TBST. Next, either the mouse anti-β-actin (1:10000) or rabbit anti-β-actin (1:1500) antibody was added in the 1% milk solution and left for 1 h at room temperature (mouse) or overnight at 4°C (rabbit). Following three washes, the appropriate horseradish peroxidase-conjugated secondary antibody (1:1000) was added to the blots in 1% milk solution and left for 1 h. The solution was removed and the membranes were developed with Immobilon Western chemiluminescent horseradish peroxidase substrate (Millipore, Billerica, MA). Band intensities were quantified using Image Lab software. All statistical analyses were performed using SigmaPlot software.

3.4 Characterization of a novel GFAT inhibitor

Previously, dehydroiso-β-lapachone was identified as a GFAT inhibitor using the Morgan-Elson assay. To further characterize this compound, assays were performed to

determine its IC_{50} and LD_{50}. For IC_{50} determination, dehydroiso-β-lapachone was added to the incubation mixture (10 mM fructose-6-phosphate (F6P) (Sigma-Aldrich), 10 mM L-glutamine (Sigma-Aldrich), 1 mM DTT, 5 mM EDTA, 1x PBS), in a 96-well plate at final concentrations from 10 nM-1 mM. GFAT activity was assessed using the Morgan-Elson assay. Briefly, the plate was sealed and heated for 1 h in a 37°C water bath. Following incubation, the GlcN-6-P produced was acetylated with 10 µl of 1.5% acetic anhydride and 50 µl of 200 mM potassium tetraborate (Sigma Aldrich). The plate was sealed with two PlateMax™ Aluminum Sealing Films (Axygen) and heated for 25 min at 80°C. After cooling for 5 min on ice, 130 µl of Ehrlich's reagent (2 g 4-dimethyl-aminobenzaldehyde, 0.3 ml ddH_2O, 2.2 ml concentrated HCl, 17.4 ml acetic acid; diluted 1:2 with acetic acid) was added to each well and the plate was incubated for 20 min at 37°C. Absorbance was measured at 585 nm on the SpectraMax Plus 384.

In the toxicity assay, dehydroiso-β-lapachone was incubated with HepG2 cells at concentrations of 0.5, 1, 10, 50 and 100 µM for 24 hrs. The percent viability was assessed on the Countess® Automated Cell Counter by mixing an equal amount of cells with Trypan Blue Stain 0.4%. Each sample was measured in duplicate.

3.5 Immunofluorescence staining

3.5.1 Tissue Sectioning

Liver used to examine the levels of GFAT and of O-GlcNAc modified proteins were obtained from two male $ApoE^{-/-}$ and two male $ApoE^{-/-}$:$Ins2^{+/Akita}$ old breeder mice. For all

other immunofluorescence experiments, livers, skeletal muscle and aortas were obtained from four male ApoE$^{-/-}$ and four male ApoE$^{-/-}$:Ins2$^{+/Akita}$ 5-month old mice **(Table 1)**. Once harvested, the tissues were immediately frozen in liquid nitrogen. Upon sectioning, the livers used for the GFAT and O-GlcNAc studies were embedded in Cryomatrix embedding resin (Thermo Scientific) and all other tissues were embedded in a modified OCT (mOCT) solution that is compatible with MALDI imaging (*75*). The mOCT solution was prepared as follows: A 10% polyvinyl alcohol (PVA) 6-98 solution was made by adding 10 g of Mowiol® 6-98 (Sigma-Aldrich) to 100 ml of Hanks' balanced salt solution (1X) (HBSS) (Life Technologies). The solution was stirred and heated until fully dissolved. Upon cooling, 8 ml of polypropylene glycol 2000 (PPG 2000) (Sigma-Aldrich) and 100 mg of sodium azide (Sigma-Aldrich) were added. The final composition of the solution was 10% (w/v) PVA 6-98, 8% (v/v) PPG 2000, 0.1% (w/v) NaN_3. The sections were cut at a 10 µm thickness and sections from two different ApoE$^{-/-}$ and two different ApoE$^{-/-}$:Ins2$^{+/Akita}$ mice were deposited onto a single slide (four sections per slide). The slides were stored at -80°C until analysis.

Table 1 | Characteristics of mice used for immunofluorescence staining, H&E staining and MALDI-IMS experiments

	Genotype	Body Weight (g)	Glucose level (mM)
$ApoE^{-/-}$ 1	$ApoE^{-/-}$	25.8	9.5
$ApoE^{-/-}$ 2	$ApoE^{-/-}$	25.9	8.1
$ApoE^{-/-}$ 3	$ApoE^{-/-}$	24.5	8.1
$ApoE^{-/-}$ 4	$ApoE^{-/-}$	24.8	7.8
Akita 1	$ApoE^{-/-}Ins2^{+/Akita}$	26.1	>32
Akita 2	$ApoE^{-/-}Ins2^{+/Akita}$	25.1	31.8
Akita 3	$ApoE^{-/-}Ins2^{+/Akita}$	23.1	>32
Akita 4	$ApoE^{-/-}Ins2^{+/Akita}$	24.2	>32

3.5.2 Staining for GFAT

Prior to staining, the tissues were fixed with ice cold acetone for 5 minutes. For all of the GFAT stains, they were then washed with 1x PBST (PBS + 0.05% TritonX-100) (3x 5 min) in order to permeabilize the cells. For the O-GlcNAc modified proteins and KDEL stains on livers and skeletal muscle tissues, the mouse on mouse (M.O.M.™) kit (Vector laboratories) was used (described below). For GFAT detection, once permeabilized, the tissues were washed with ddH_2O (2x 5 min) followed by PBST (2x 5 min). To block non-specific binding of the antibodies, 10% goat serum in PBST was added to the tissues and was left on for 2 hours. The primary antibodies [rabbit polyclonal GFAT (1:50, Santa Cruz Biotechnology), rabbit polyclonal IgG (1:1250, Invitrogen)] were added next in 10% blocking serum and left on overnight at 4°C. Following 3 washes with PBS (5 min each), the 2° antibody [Alexa Fluor® 594 goat anti-rabbit IgG (1:300; Invitrogen)] was added in PBS and left for 1 hour at room temperature. The slides were then washed with PBS (3x 5 min) and ddH_2O (2x 5 min). To stain nuclei, 4',6-diamidino-2-phenylindole (DAPI) was

added for 2 minutes. After three final washes with ddH_2O (5 min) one drop of Fluoromount™ Aqueous Mounting Medium (Sigma-Aldrich) was added onto each tissue section and a coverslip was placed on top prior to obtaining fluorescent images at 4, 10 and 20x magnification. The images were analyzed using ImageJ software. For all measurements, the fluorescence intensity of the target signal was normalized to that of the DAPI signal. All t-tests used for statistical analyses were performed using SigmaPlot software.

3.5.3 Staining for O-GlcNAc modified proteins and KDEL

For the O-GlcNAc modified proteins and KDEL stains, the M.O.M.™ kit staining procedure for frozen sections was followed. Briefly, after fixing the tissues with ice cold acetone for 5 minutes, the sections were left to air dry. Next, they were washed 2x 2 min with PBS and incubated for 1 hour in a working solution of M.O.M.™ Mouse Ig Blocking Reagent prepared by adding 90 µl of the stock solution to 2.5 ml of PBS. Following 2 washes with PBS (2 min each) the tissues were incubated for 5 minutes in a working solution of M.O.M.™ Diluent prepared by adding 600 µl of the Protein Concentrate stock solution to 7.5 ml of PBS. The primary antibodies [O-GlcNAc antibody (mouse monoclonal RL2) (1:200, Affinity Bioreagents Inc.), mouse monoclonal anti-KDEL (1:95, Stressgen), normal mouse IgG (1:250, Invitrogen)] were diluted in the M.O.M.™ Diluent prepared above and incubated with the sections for 45 minutes. After 2 washes with PBS (2 min each) a working solution of M.O.M.™ Biotinylated Anti-Mouse IgG

Reagent was prepared by adding 10 µl of stock solution to 2.5 ml of prepared M.O.M.™ Diluent and incubated with the sections for 10 minutes. Following another 2x 2 min PBS washes the secondary streptavidin-linked fluorescent antibody [Alexa Fluor® 594 (1:5000; Molecular Probes)] was added and left on sections for 30 minutes. After 2x 2 min washes with PBS, DAPI was added for 1 min, the sections were washed again with PBS (2x 5 min) and mounted in Fluoromount™ Aqueous Mounting Medium prior to obtaining images.

3.5.4 Paraffin-embedded sections

Due to an extremely high background signal coming from the frozen aortic sections, even when using the M.O.M.™ kit, paraffin-embedded sections from two male ApoE$^{-/-}$ and two male ApoE$^{-/-}$:Ins2$^{+/Akita}$ were obtained from Daniel Venegas-Pino and used for detecting O-GlcNAc modified proteins and KDEL. The sections were placed in an air heater for 8 minutes to melt the paraffin. They were then deparaffinized and hydrated by sequential dips in xylenes (4x 4 min), 100% ethanol (3x 4 min), 70% ethanol (2x 4 min), 50% ethanol (2x 4min) and dH_2O (5 min). Antigen retrieval was performed next by first preparing a solution of 1.6 L dH_2O and 15 ml of antigen unmasking solution (Vector Laboratories) in a microwave-safe bowl and heating on high power, uncovered, for 17 minutes. The slides were then placed into the solution and the container was sealed with a lid. The container was heated for 3 min then left to cool to room temperature. The slides were removed from the solution and placed in dH_2O, followed

by washing with PBS for 5 min. The M.O.M.™ kit was used, as described above, for the staining procedure beginning with the addition of the Mouse Ig Blocking Reagent.

3.6 MALDI-Imaging Mass Spectrometry

The preparation and imaging of liver sections was performed by The Centre for the Study of Complex Childhood Diseases, The Hospital for Sick Children, Toronto, Canada. All other imaging was performed at the Biointerfaces Institute at McMaster University. Liver, skeletal muscle and heart specimens were frozen rapidly to -20°C. The tissues were embedded in mOCT (except for the liver, which was not embedded in any medium), cut in 10 µm (12 µm for liver) sections and mounted onto indium tin oxide (ITO)-coated glass slides. They were then sprayed with a 9-aminoacridine matrix solution (Sigma-Aldrich) using an automated MALDI plate matrix deposition system (TM-Sprayer™, Leap Technologies', Carrboro, NC). A total of 5 mL of 9-aminoacridine solution (15 mg/mL in methanol) was applied per slide during 4 passes at 80°C with a velocity of 400 mm/min and a line spacing of 3 mm. A time-of-flight tandem mass spectrometer (AB Sciex TOF/TOF™ 5800 System, AB SCIEX, Ontario, Canada) was used to acquire the images of the liver sections, and the Bruker MALDI-TOF/TOF ultrafleXtreme system was used to acquire the images of the skeletal muscle and aortic sections. MALDI mass spectra were obtained using an Nd:YAG laser (349 nm) at 3 ns pulse width and 400 Hz firing rate. All data were acquired in the negative-ion reflector mode within the mass ranges of m/z 400–1200. Aliquots of UDP-N-acetylglucosamine were deposited on the

ITO-coated slides as an external standard and to compensate for mass shift. Phosphatidylinositol (PI) 18:0/20:4 (m/z 885.5) was used as a calibrant and an internal control to show the structure of the tissue. A total of 200 laser shots per pixel were acquired (1 s/pixel) at a spacing of 75 µm between pixels. The mass spectrometric data for the livers was processed and images were visualized using TissueView software (AB SCIEX), while the skeletal muscle and aortic images were processed and visualized using the Fleximaging 4.0 Software (Bruker).

3.7 H&E staining

Following imaging by MALDI-IMS, the slides were washed in 70% ethanol (2x1 min) then in 100% ethanol (2x1 min) to remove the matrix solution. The slides were left to air dry at room temperature before proceeding with the staining. Once dried, the tissues were stained with 0.1% Meyer's hematoxylin solution for 3 minutes, and then were rinsed in cool running ddH_2O for 5 minutes. Next, the tissues were counterstained with a 0.5% eosin solution for 1 min. After 3 washes with ddH_2O (5 min each), the slides were dipped in 50%, then 70% ethanol 10x each. Following equilibration in 100% ethanol (3x1 min), the slides were dipped in xylene (4x1 min). A few drops of xylene mounting medium were then added onto each slide and a coverslip was placed on top prior to obtaining images.

CHAPTER 4. RESULTS

4.1 Development of the HPLC-MS system for monitoring UDP-GlcNAc levels

In order to directly monitor the effects of HBP modulators in cell lysates and in tissues, an HPLC-MS system was established. This method was adapted from the one developed by Chalcraft et al., who demonstrated that the use of a ZIC-HILIC column along with a gradient elution series results in effective separation of polar compounds (*76*). Prior to analysis by HPLC-MS, a sample preparation protocol was developed (**Figure 7**). Once prepared, the mixture was run through the HPLC-MS system where HPLC chromatograms and mass spectra were obtained (**Figure 8**). This system allows us to compare the levels of the end product of the HBP, UDP-GlcNAc, in various treatment groups. The internal standard used is the dipeptide Gly-Phe, which was added to each cell lysate sample in order to correct for any sample loss during the sample preparation stage. The peak representing UDP-GlcNAc was confirmed with a standard, which eluted with the same retention time as the peak seen in the samples.

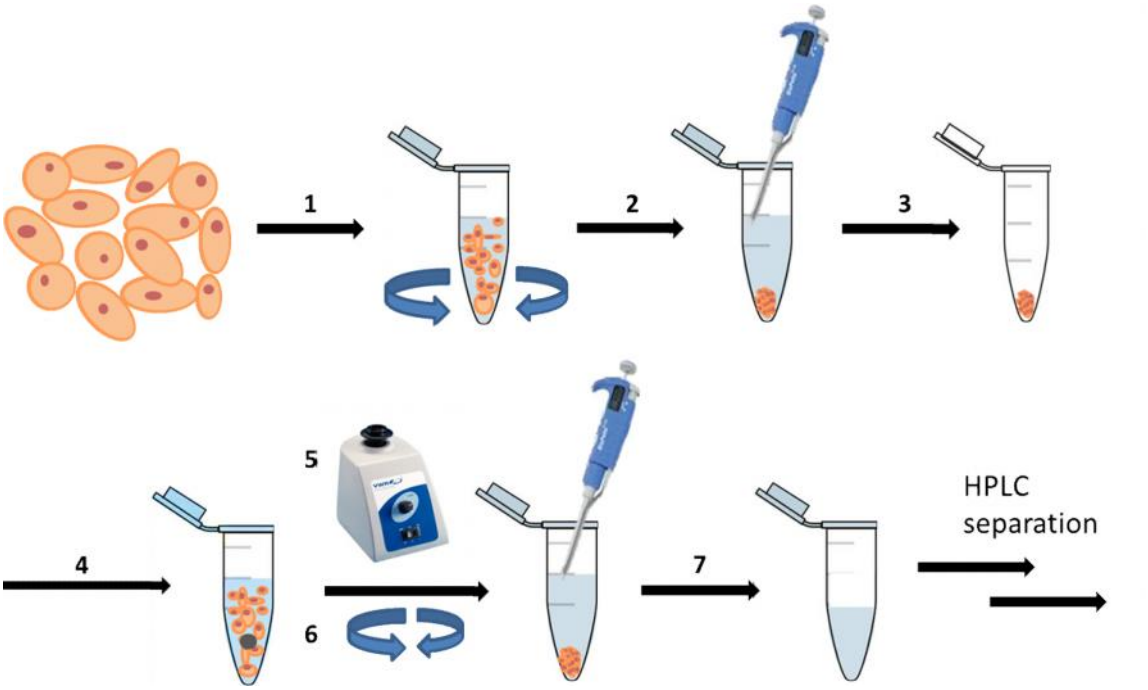

Figure 7 | Sample preparation steps prior to HPLC analysis for cultured cells. 1. Harvest cells*; 2. Spin down cells; 3. Remove supernatant; 4. Add extraction solvent(s) containing internal standard (Gly-Phe) and small metal bead to cells; 5. Vortex to lyse cells; 6. Remove bead and spin down cells; 7. Collect supernatant containing molecules of interest for HPLC separation.
*At this point a portion of the cell solution was removed and used for cell counting for normalization of results.

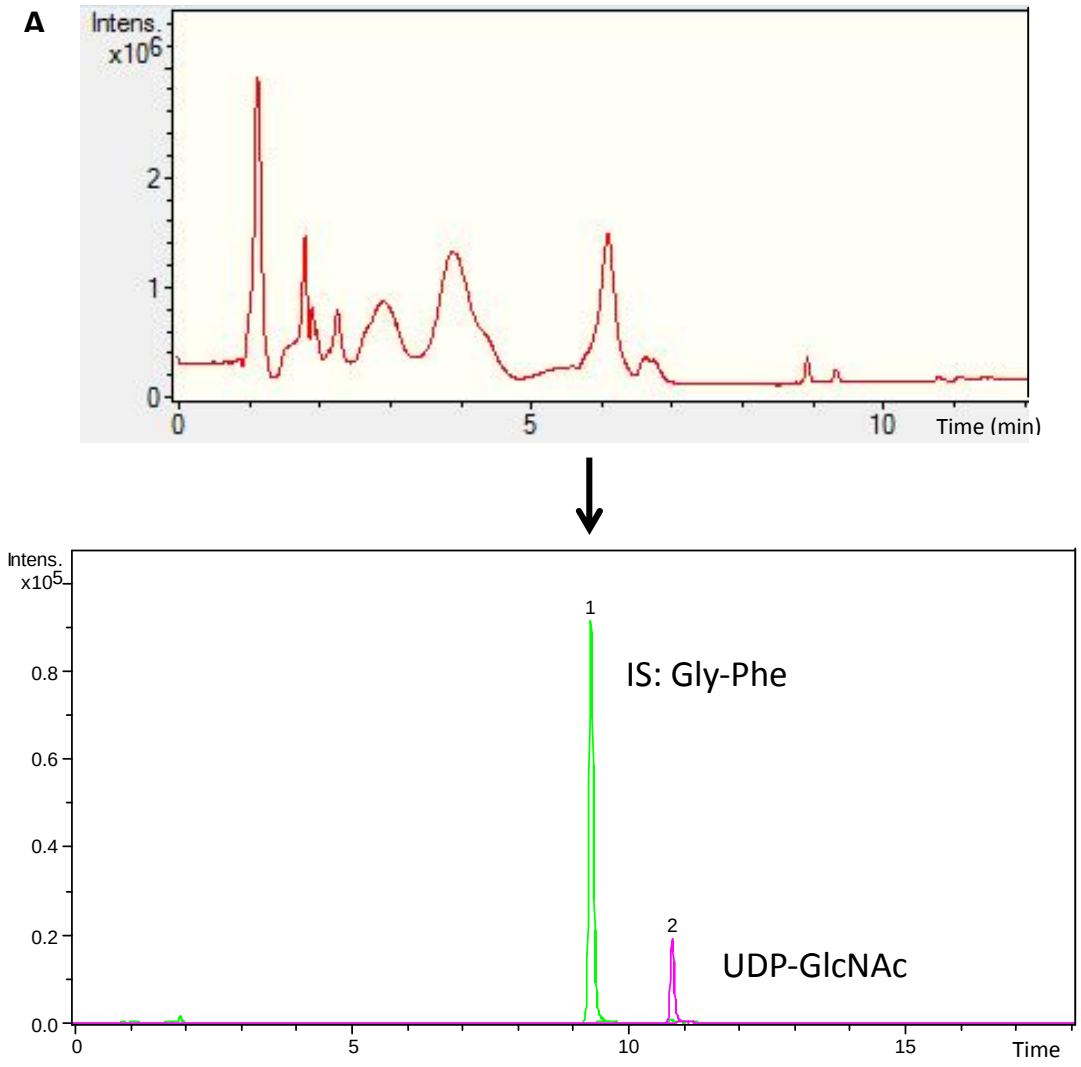
A
Intens.
x10^6
2
1
0
0
5
10
Time (min)
Intens.
x10^5
0.8
0.6
0.4
0.2
0.0
1
IS: Gly-Phe
2
UDP-GlcNAc
0
5
10
15
Time

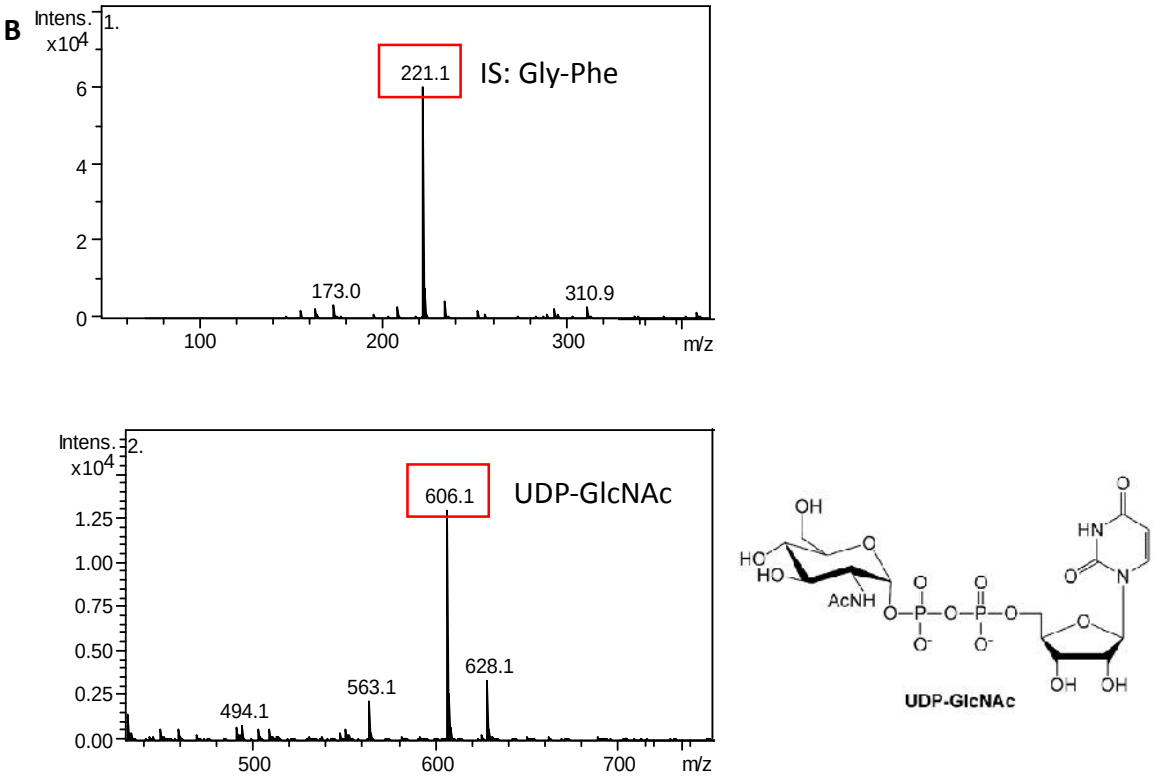

Figure 8 | Analysis of a cell lysate sample by HPLC-MS. A) Original and processed HPLC chromatograms, where peak 1 represents the internal standard Gly-Phe (m/z 221.1) added to the sample and peak 2 represents UDP-GlcNAc (m/z 606.1) in the cell lysate. B) Corresponding mass spectra of the peaks shown in the processed HPLC chromatogram.

4.2 Stimulating the HBP: effects on UDP-GlcNAc levels and ER stress

4.2.1 Glucosamine increases HBP flux and triggers ER stress in cultured cells

To determine the effects on HBP metabolites from glucose and glucosamine supplementation, HepG2 cells and L6 rat skeletal muscle cells were treated with the sugars for 24 hours prior to harvesting and the levels of UDP-GlcNAc relative to an internal standard in each sample was determined by HPLC-MS. Although glucose supplementation did not appear to have an effect on HBP flux in either cell type, treatment with glucosamine did in a dose-dependent manner, with UDP-GlcNAc levels

increasing between 4 and 10 fold relative to the control in HepG2 cells (**Figure 9a**), and over 45-fold with 5 mM glucosamine in the skeletal muscle cells (**Figure 9b**). To assess the ability of glucosamine to induce ER stress, HepG2 cells were treated with glucosamine at various concentrations (0.2-5 mM) and harvested at various time points (2-18 h). The lysates were resolved by SDS-PAGE and immunoblotted with an antibody against the ER retention sequence (KDEL) that identifies the ER chaperone proteins and established ER stress markers, Grp78 and Grp94. The expression levels of both proteins increased in both concentration and time-dependant manners, relative to the β-actin levels in each sample (**Figure 10**).

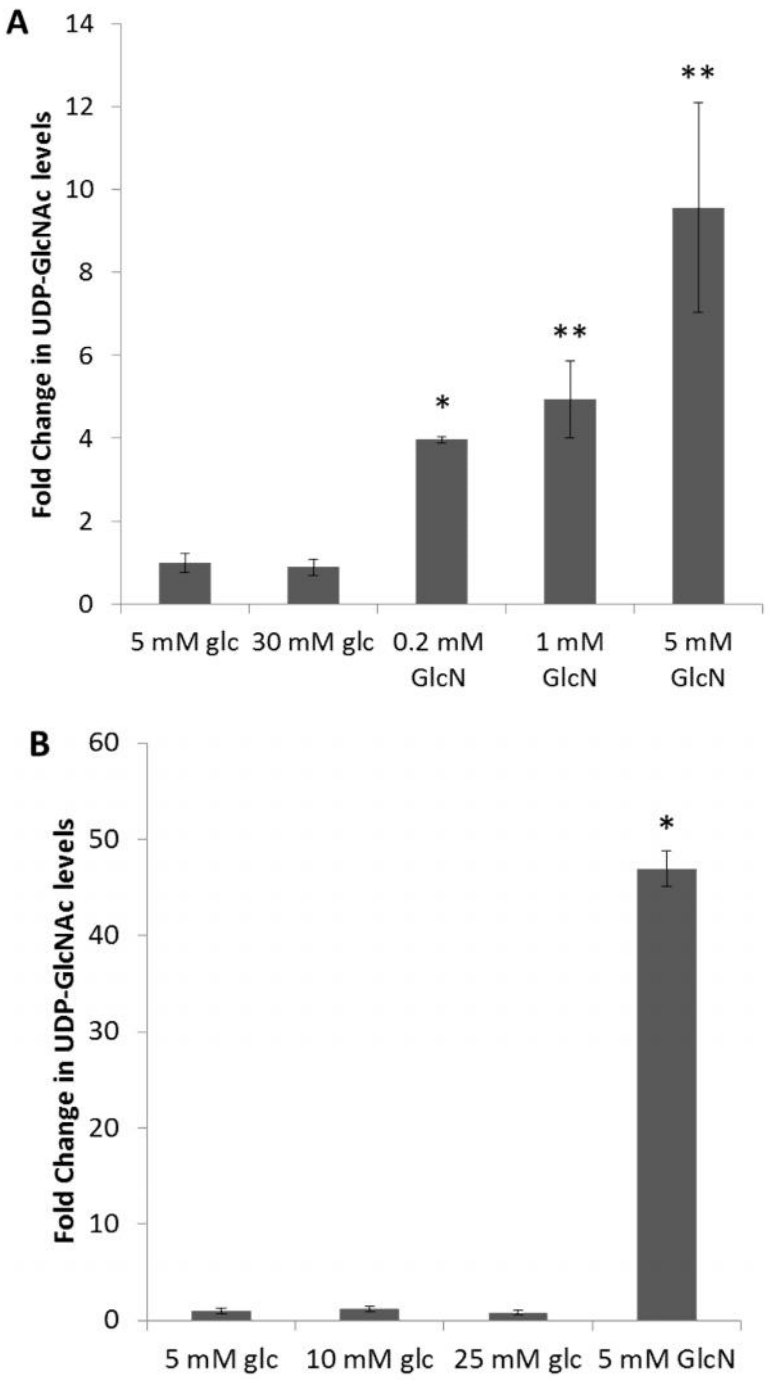

Figure 9 | Fold change in UDP-GlcNAc levels in different cell types in response to glucose (glc) or glucosamine (GlcN) treatment. A) UDP-GlcNAc levels in HepG2 cells relative to the internal standard (RRF) and normalized to the amount of cells in each sample (**P*<0.05 relative to 5 mM glc, n=4) (***P*<0.001 relative to 5 mM glc, n=5). B) UDP-GlcNAc levels in L6 rat skeletal muscle cells (**P*<0.001 relative to 5 mM glc, n=4).

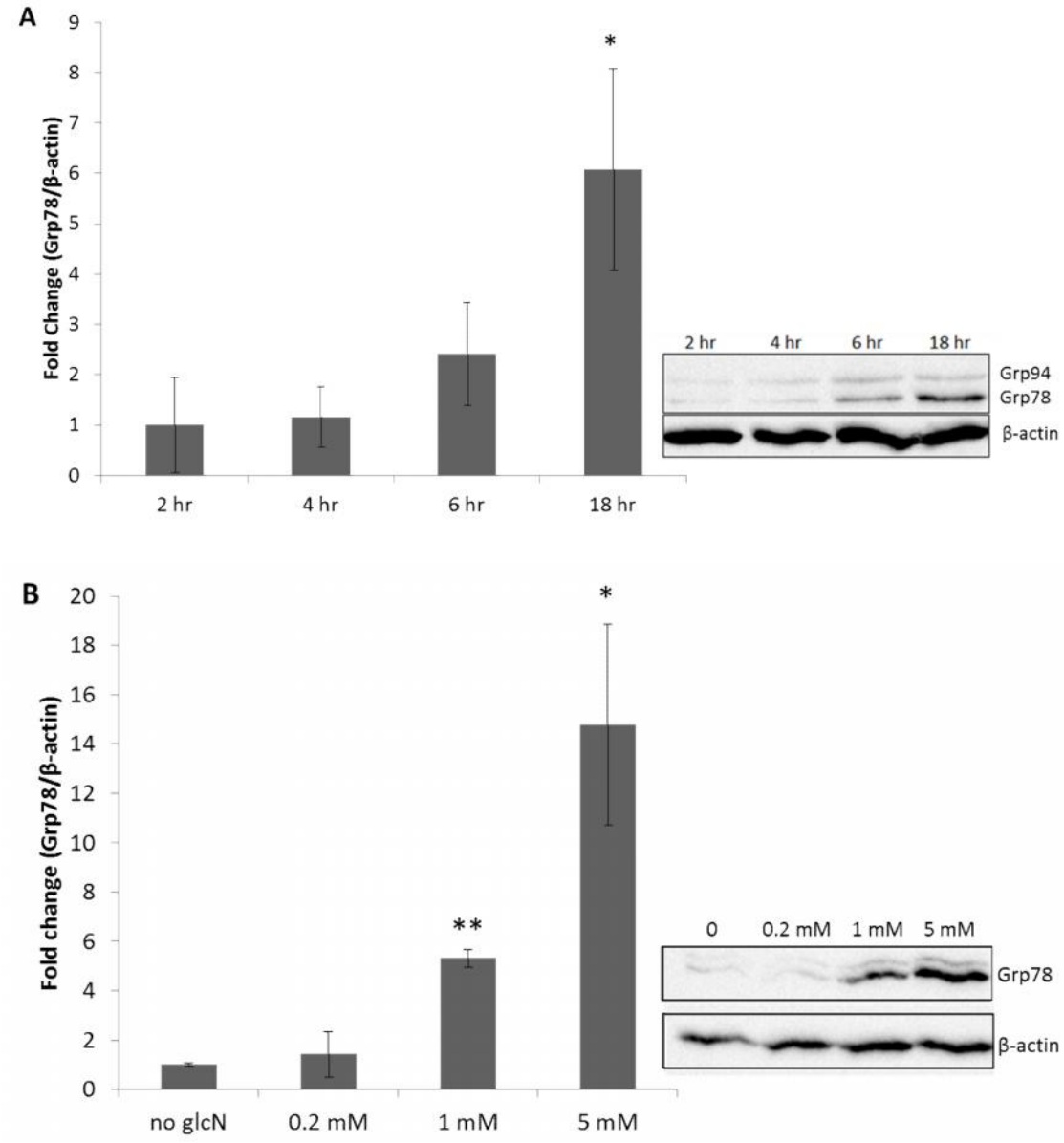

Figure 10 | **Effect of glucosamine on levels of the ER chaperone protein Grp78.** (A) Grp78 levels relative to β-actin levels in HepG2 cells treated with 1 mM glucosamine for 24 h. (**P*<0.05 relative to 2 hr treatment, n=2). (B) Grp78 levels relative to β-actin levels in HepG2 cells treated with glucosamine at various concentrations. (**P*<0.05, ***P*<0.005 relative to no glcN, n=2).

4.2.2 GFAT overexpression causes increased HBP flux

GFAT was overexpressed in HepG2 cells using an adenovirus (**Figure 11a**).

Previously, the ideal multiplicity of infection (MOI), which is the ratio of virus particles to

cells, required to achieve overexpression was determined to be 25. Successful infection was confirmed by observing fluorescence from GFP (**Figure 11b**). Overexpression of GFAT was confirmed through a Western blot, and was only observed in cells treated with the adenovirus (**Figure 11c**). To test the effects of GFAT overexpression on HBP flux, UDP-GlcNAc levels were compared in cells infected with the adenovirus containing a gene encoding GFAT to those infected with a control adenovirus (Ad-GFP). The results show that UDP-GlcNAc levels were increased 7-fold in cells overexpressing GFAT (**Figure 12**).

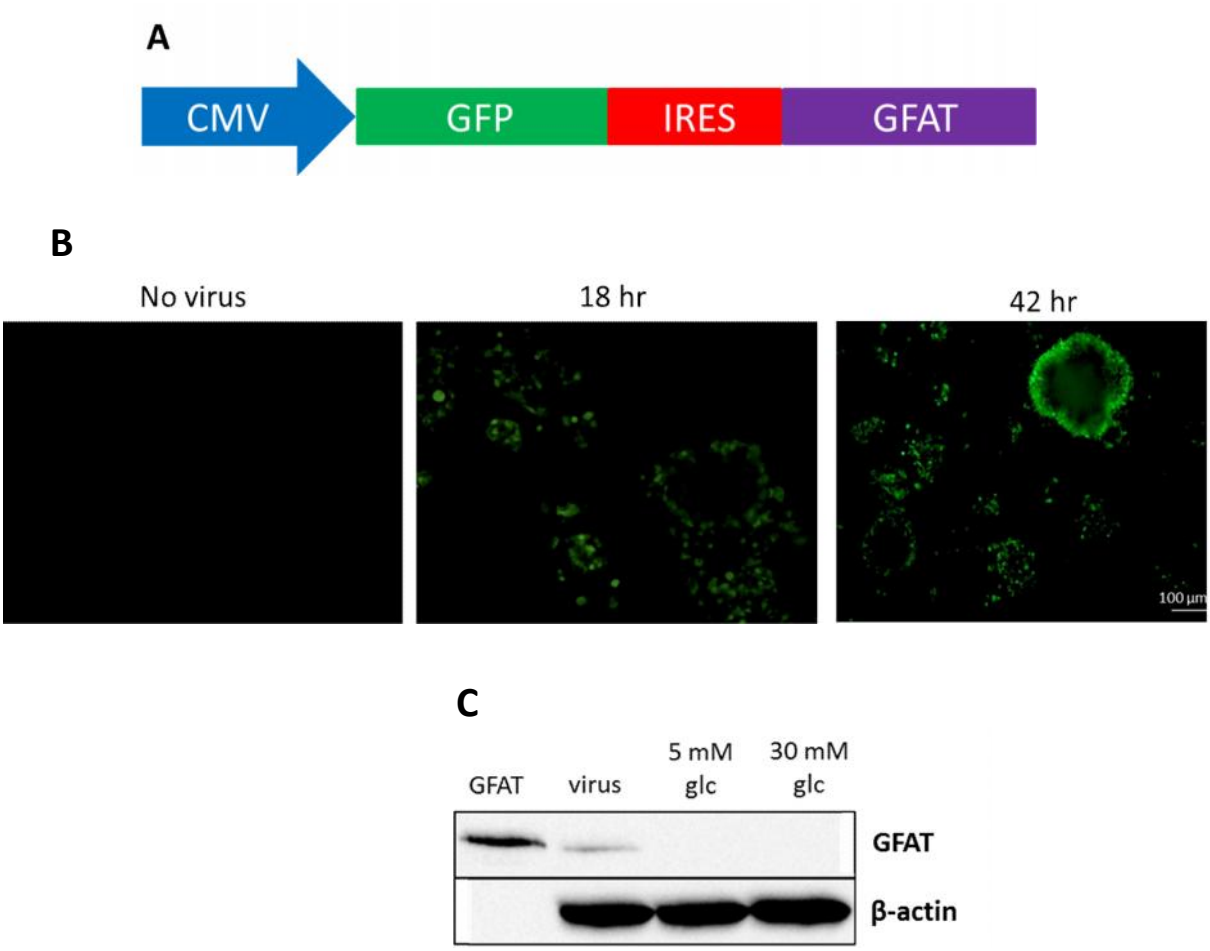

Figure 11 | Overexpression of GFAT using an adenoviral system. (A) Arrangement of genes in adenovirus used to overexpress GFAT; CMV=cytomegalovirus promoter, IRES=internal ribosomal entry sequence. (B) Fluorescence over time in HepG2 cells treated with Ad-GFP-GFAT at an MOI of 25. (C) Immunoblot analysis of GFAT expression (77 kDa). Samples were treated with either the adenovirus overexpressing GFAT, low (5 mM) glucose or high (30 mM) glucose. Affinity purified recombinant human GFAT, purified by Lisa Walter was run as a control.

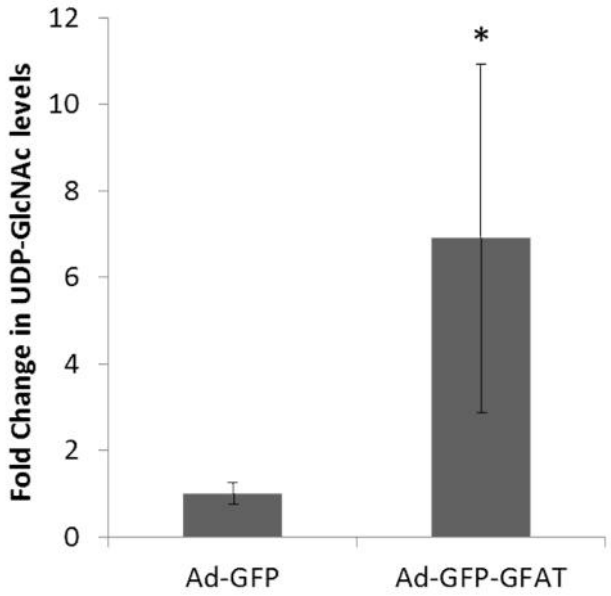

Figure 12 | UDP-GlcNAc levels in HepG2 cells overexpressing GFAT. Values are normalized to the peak internal standard and cell count. *P<0.05 relative to cells infected with control adenovirus. n=5 for Ad-GFP and n=4 for Ad-GFP-GFAT.

4.3 Attenuating the HBP: effects on UDP-GlcNAc levels and ER stress

4.3.1 GFAT inhibitors lower UDP-GlcNAc levels

Three of the compounds identified as GFAT inhibitors *in vitro* were tested for their inhibitory activity in cultured cells by HPLC-MS. This work was performed in collaboration with Lisa A. Walter, who initially identified the inhibitors *in vitro* (*51*). HepG2 cells were treated with these compounds at three concentrations (10, 20 and 50 µM) two hours prior to harvesting. Their ability to decrease HBP flux was evaluated by determining the levels of UDP-GlcNAc in treated samples relative to controls that did not contain an inhibitor. Cells treated with 20 µM and 50 µM of amrinone showed a significant decrease in UDP-GlcNAc levels compared to the control (P<0.05) (**Figure 13**). Similar results were observed in lapachol-treated cells, where UDP-GlcNAc levels were

decreased nearly 2 and 3-fold compared to the control for 20 µM and 50 µM treatments, respectively (P<0.05) (**Figure 13**). Cells treated with alloxan showed significant decreases in UDP-GlcNAc levels at all inhibitor concentrations relative to the control (P<0.05 for 10 µM and P<0.001 for 20 µM and 50 µM) (**Figure 13**).

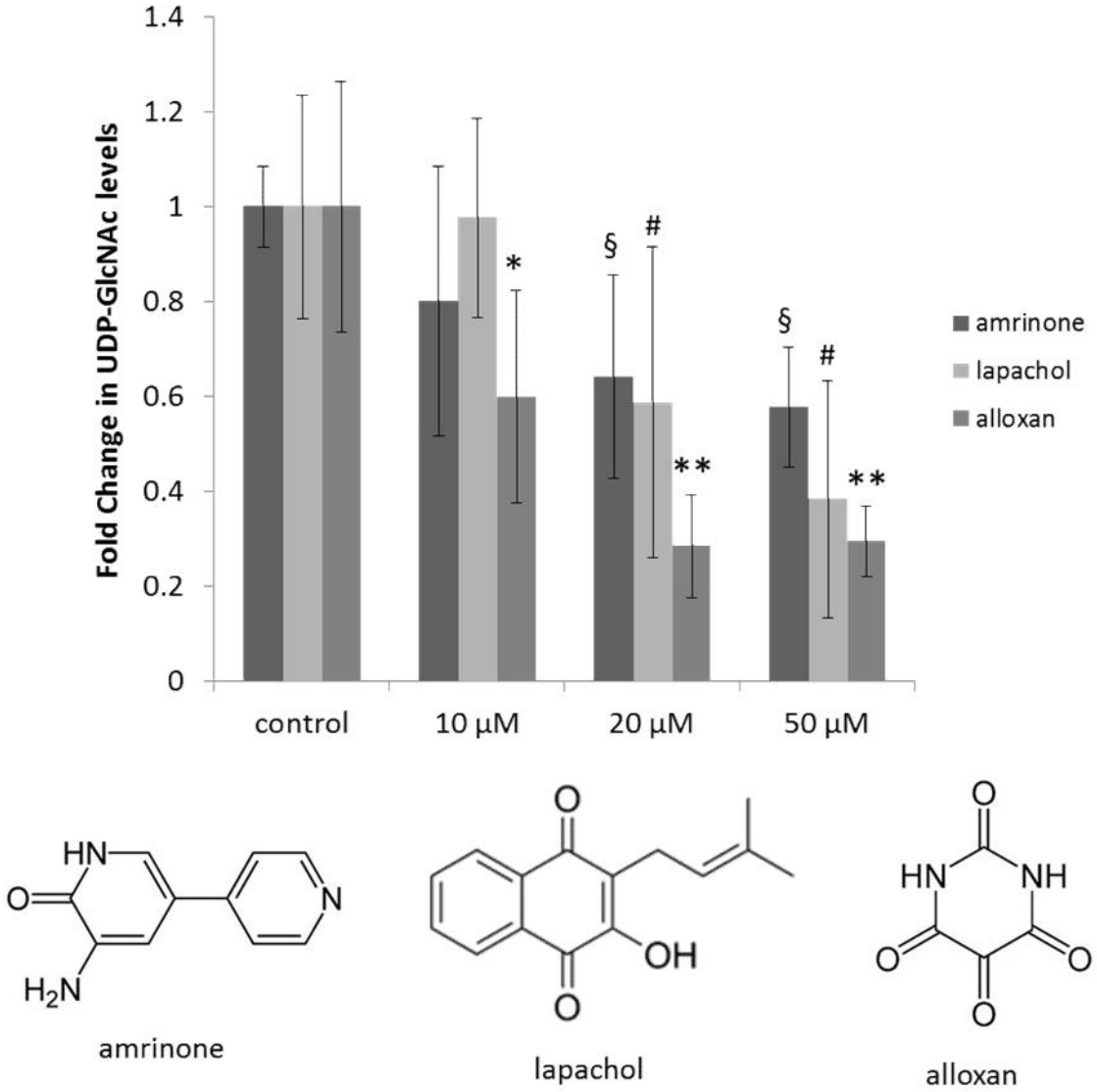

Figure 13 | Effects of GFAT inhibitors on UDP-GlcNAc levels. UDP-GlcNAc levels in HepG2 cells treated with (A) amrinone (§*P* <0.05 relative to control, n=5, 3 for 20 µM and 50 µM, respectively), (B) lapachol (#*P*<0.05 relative to control, n=5) and (C) alloxan (**P*<0.05 relative to control, n=5) (***P*<0.001 relative to control, n=4, 6 for 20 µM and 50 µM, respectively).

4.3.2 Identification of a novel GFAT inhibitor

A novel GFAT inhibitor containing the naphthoquinone core has been identified using the Morgan-Elson assay. This work was performed in collaboration with Lisa A. Walter (*51*). This compound, dehydroiso-β-lapachone (**Figure 14a**), was further characterized in terms of its inhibitory potency and degree of toxicity, and the IC_{50} and LD_{50} were determined to be 1.9 ± 0.2 µM and 73 µM, respectively (**Figure 14**). This translates to a therapeutic ratio of 38:1.

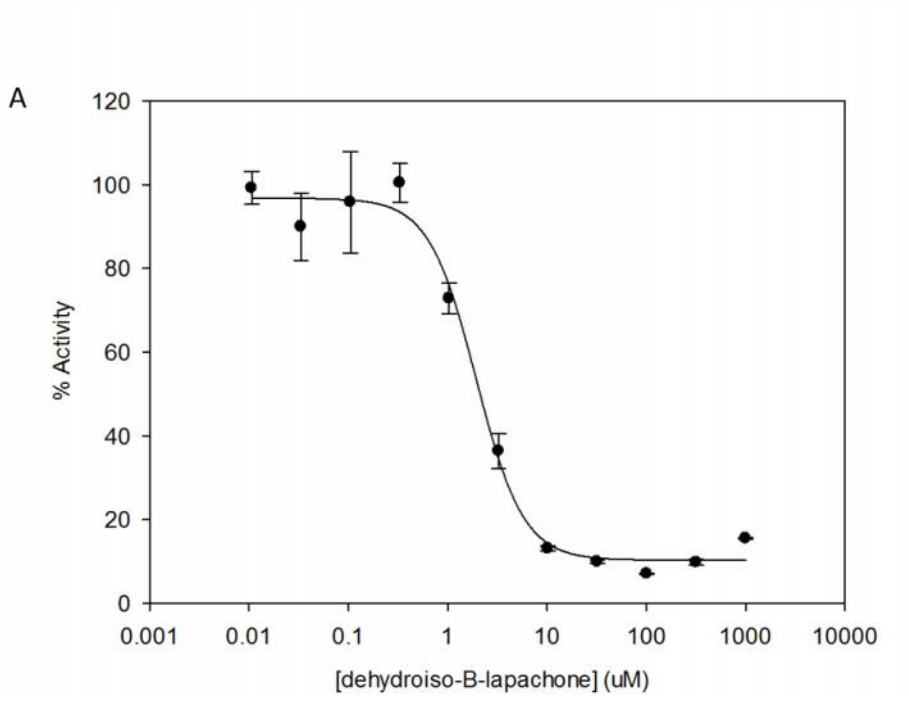

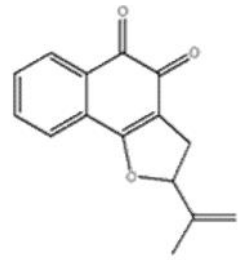

Dehydroiso-β-lapachone

B

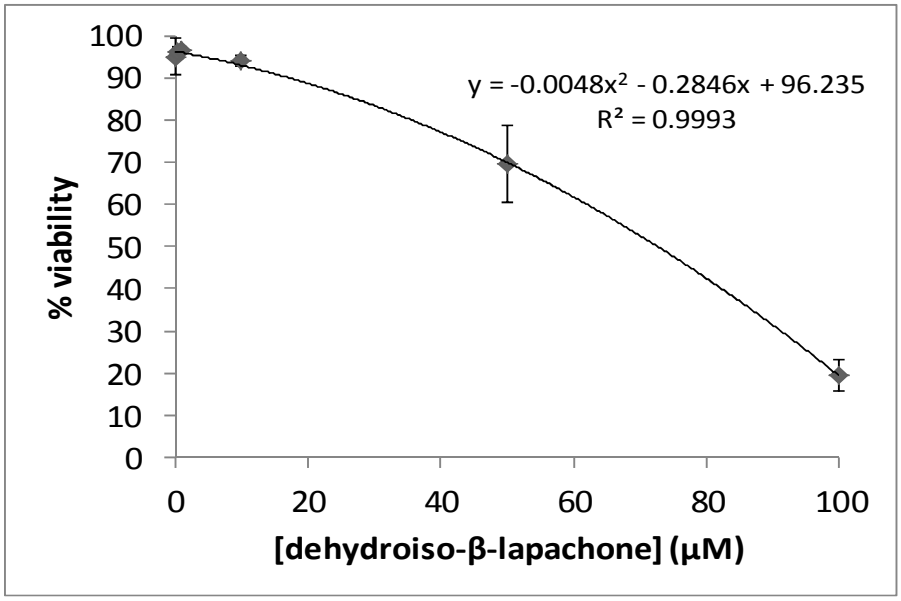

Figure 14 | Characterization of inhibitory properties and toxicity of dehydroiso-β-lapachone. A) IC_{50} curve for dehydroiso-β-lapachone against GFAT; IC_{50} = 1.9 ± 0.2 μM; n=3. Structure of compound shown in the right. B) Effect of dehydroiso-β-lapachone on HepG2 cell viability; LD_{50} = 73 μM; n=2.

4.3.3 Dehydroiso-β-lapachone attenuates the ER stress response

The effect of dehydroiso-β-lapachone on the ER stress response was examined. Cells infected with Ad-GFP-GFAT and treated with the compound at a concentration of 20 μM showed decreased levels of the ER chaperone protein, Grp94, at 3, 5 and 7 hours post-treatment (**Figure 15**). These levels even were lower than those of uninfected cells. In an attempt to increase flux through the HBP in order to more accurately assess the

abilities of the inhibitors to revert the flux back to normal levels, three cell types – HepG2, MOVAS and THP-1 cells – were treated with ATP and citrate. Although a slight increase in the levels of the p62-O-GlcNAc protein was observed, suggesting increased HBP flux, the results were inconsistent between separate experiments and the overall increase in flux was not to a level high enough to accurately assess the inhibitors' abilities to prevent this increase (**Figure 16**). Higher concentrations of citrate and longer time points were also tested, and the mRNA levels of ER stress proteins were examined, however a significant increase in flux through the HBP could not be achieved by any of these means (data not shown).

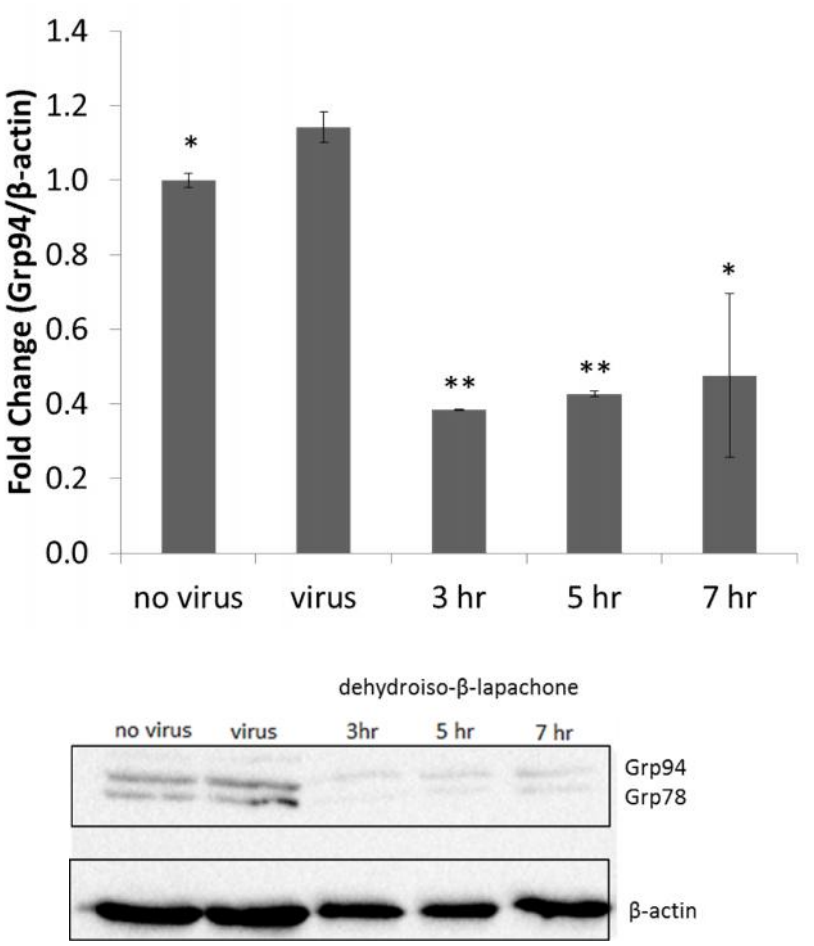

Figure 15 | Effect of the GFAT inhibitor dehyroiso-β-lapachone on ER stress. Grp94 levels relative to β-actin levels in HepG2 cells treated with Ad-GFP-GFAT and 20 µM dehydroiso-β-lapachone over time (**P* < 0.05, ***P* < 0.001 relative to virus alone, n=2).

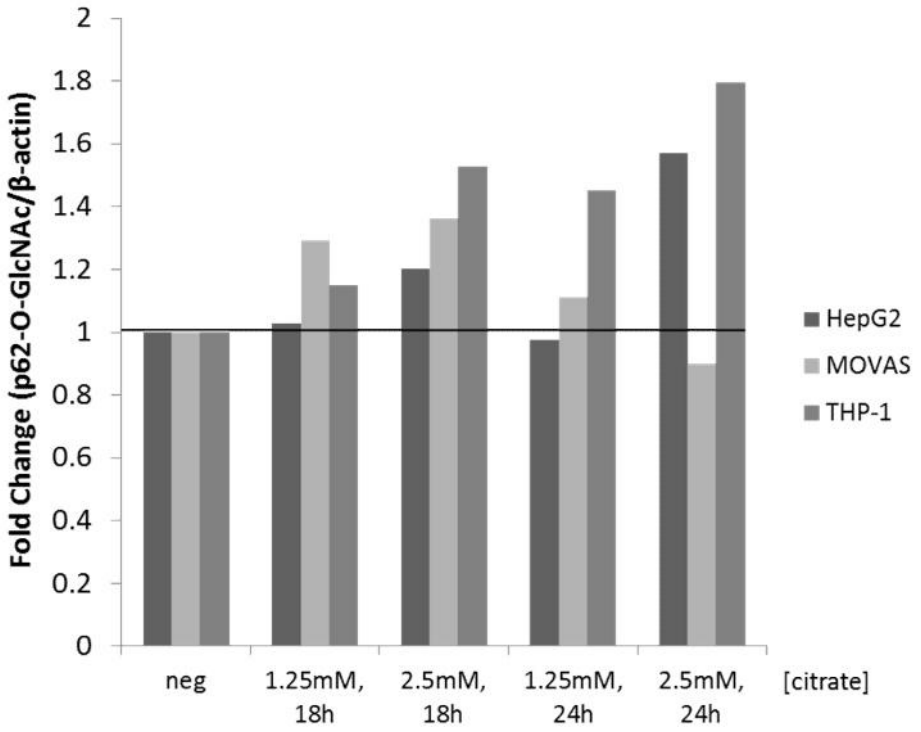

Figure 16 | Increasing HBP flux using citrate and ATP. p62-O-GlcNAc levels in HepG2, MOVAS and THP-1 cells treated with 1.75 mM ATP and either 1.25 or 2.5 mM citrate, at 18 and 24 hours.

4.4 In vivo effects of HBP stimulation by hyperglycemia and glucosamine treatment

4.4.1 Expanding the HPLC-MS system

To explore the utilities of the HPLC-MS system beyond the analysis of cultured cells, human blood and mouse liver tissues were extracted and analyzed using this technique. As shown in **figures 17 and 18**, UDP-GlcNAc could be detected in both human blood and in mouse liver, suggesting that this method could be used for further investigation of the effects of hyperglycemia on HBP flux in various different tissues. Ingestion of a glucose drink (75 g) did not seem to have an effect on HBP flux in blood samples of a healthy individual, 2 and 4 hours following glucose consumption (**Figure**

17). The individual's blood glucose levels at each time point were as follows: 4.5 mM at t=0, 5.2 mM at t=2, and 5.6 mM at t=4. Increased flux through the HBP (1.5-fold) was observed in the livers of mice supplemented with 5% glucosamine in their drinking water, however this trend was not observed in the hyperglycemic Akita mice (**Figure 18**).

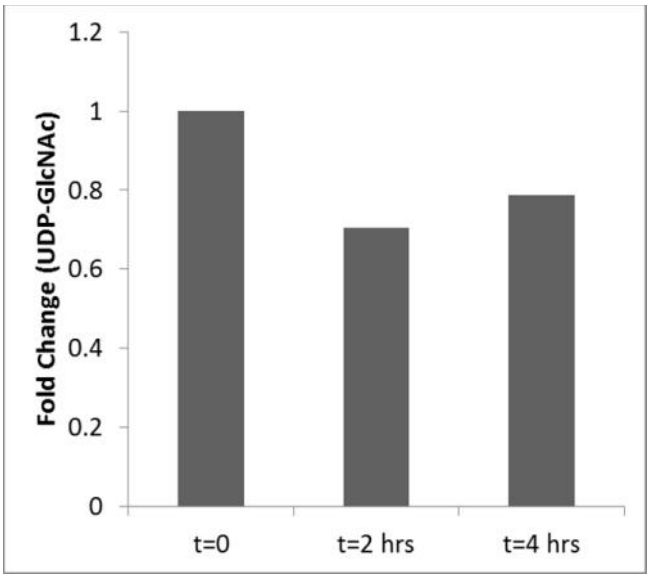

Figure 17 | UDP-GlcNAc levels in human blood following glucose consumption. UDP-GlcNAc levels in a healthy individual's blood measured before ingestion of a glucose drink (75 g glucose) in the fasting state (t=0), and 2 and 4 hours following the drink. Equal volumes (10 mL) of blood were used for each sample (n=1).

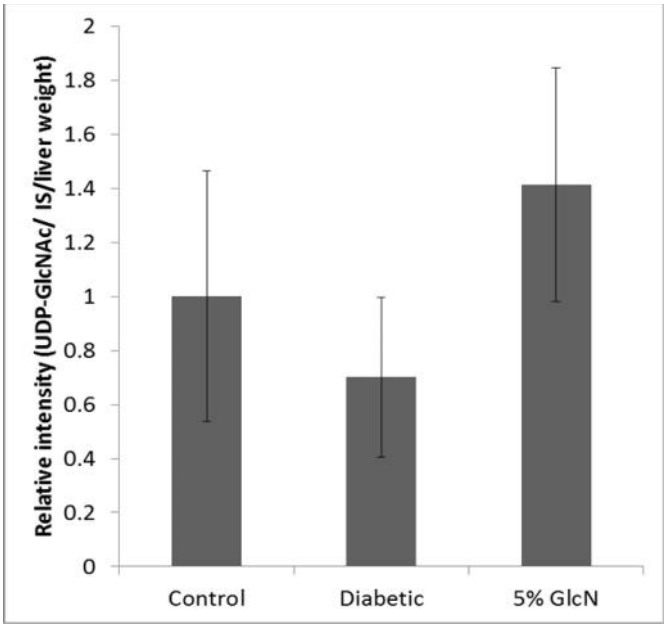

Figure 18 | UDP-GlcNAc levels in mouse liver tissue. UDP-GlcNAc levels relative to the internal standard and normalized to liver weight in livers of male control ($ApoE^{-/-}$), diabetic ($ApoE^{-/-}Ins2^{+/Akita}$), and 5% GlcN ($ApoE^{-/-}$ with 5% glucosamine added to drinking water) mice at 25 weeks of age (n=3 for control and diabetic, n=2 for 5% GlcN).

4.4.2 Effects of hyperglycemia in liver

Both GFAT expression and levels of O-GlcNAc-linked proteins were elevated (2.6-fold and 2.1-fold, respectively) in the livers of mice containing a point mutation in the Ins2 gene relative to mice lacking this mutation as determined through immunofluorescence staining (**Figure 19**). The reason for these differences in Akita mice is unclear; however in the context of hyperglycemia we would anticipate a significant increase in HBP flux due to their extreme hyperglycemic state. Recent evidence from our lab shows that these mice develop downstream complications associated with diabetes including hepatic steatosis and increased atherosclerotic lesion size, suggesting a link between increased HBP flux and accelerated development of atherosclerosis. The

MALDI-IMS image also shows evidence of an augmented HBP in the liver of an Akita mouse relative to an ApoE$^{-/-}$ control (**Figure 20**).

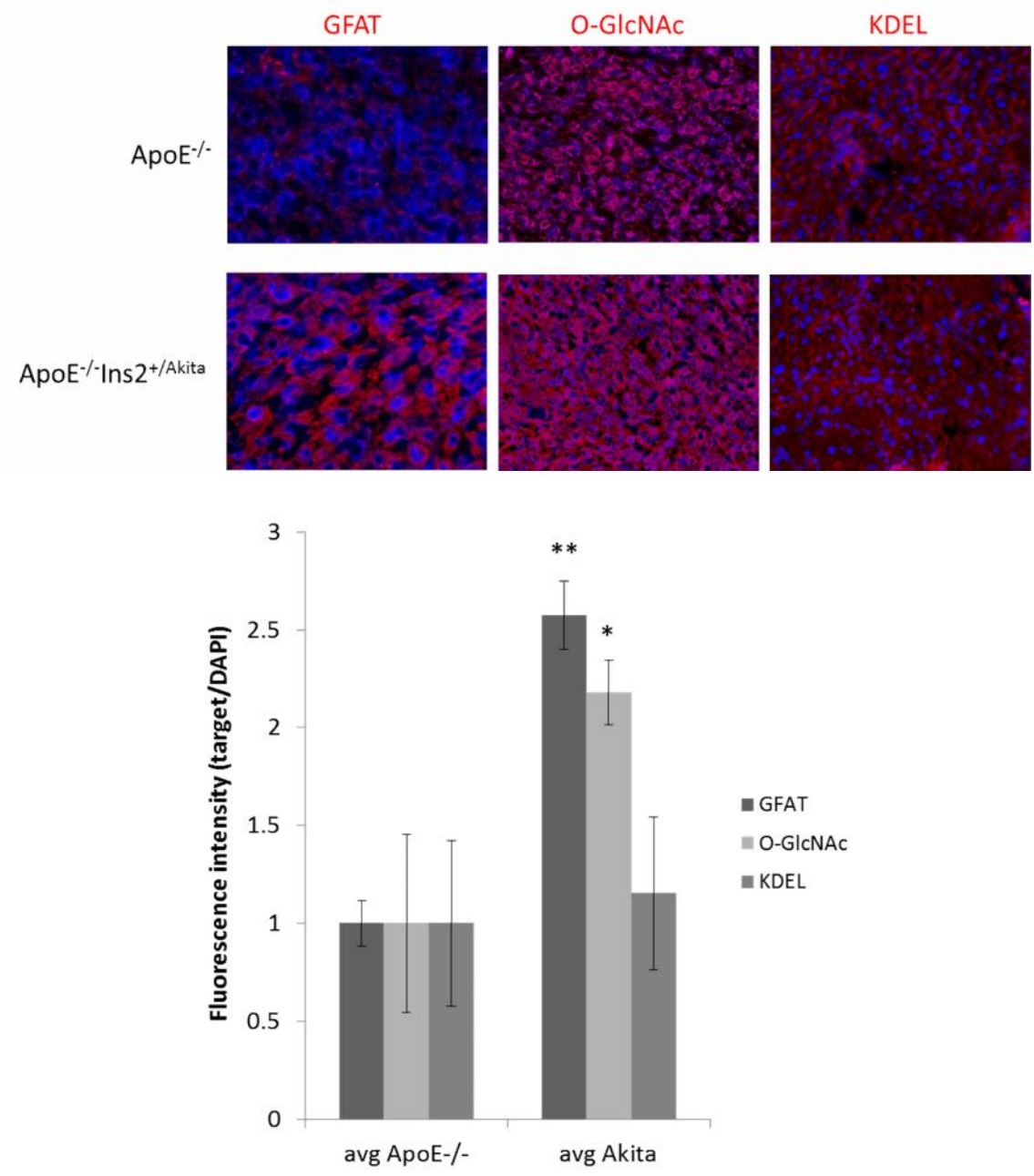

Figure 19 | Immunofluorescence analysis of liver tissue. IF images of liver sections from male ApoE$^{-/-}$ and ApoE$^{-/-}$:Ins2$^{+/Akita}$ mice showing GFAT, O-GlcNAc modified proteins or proteins containing the KDEL sequence in red (blue=DAPI). The normalized fluorescence intensity is quantified below. ***P*<0.005, **P*<0.05; n=2 for GFAT and O-GlcNAc, n=4 for KDEL.

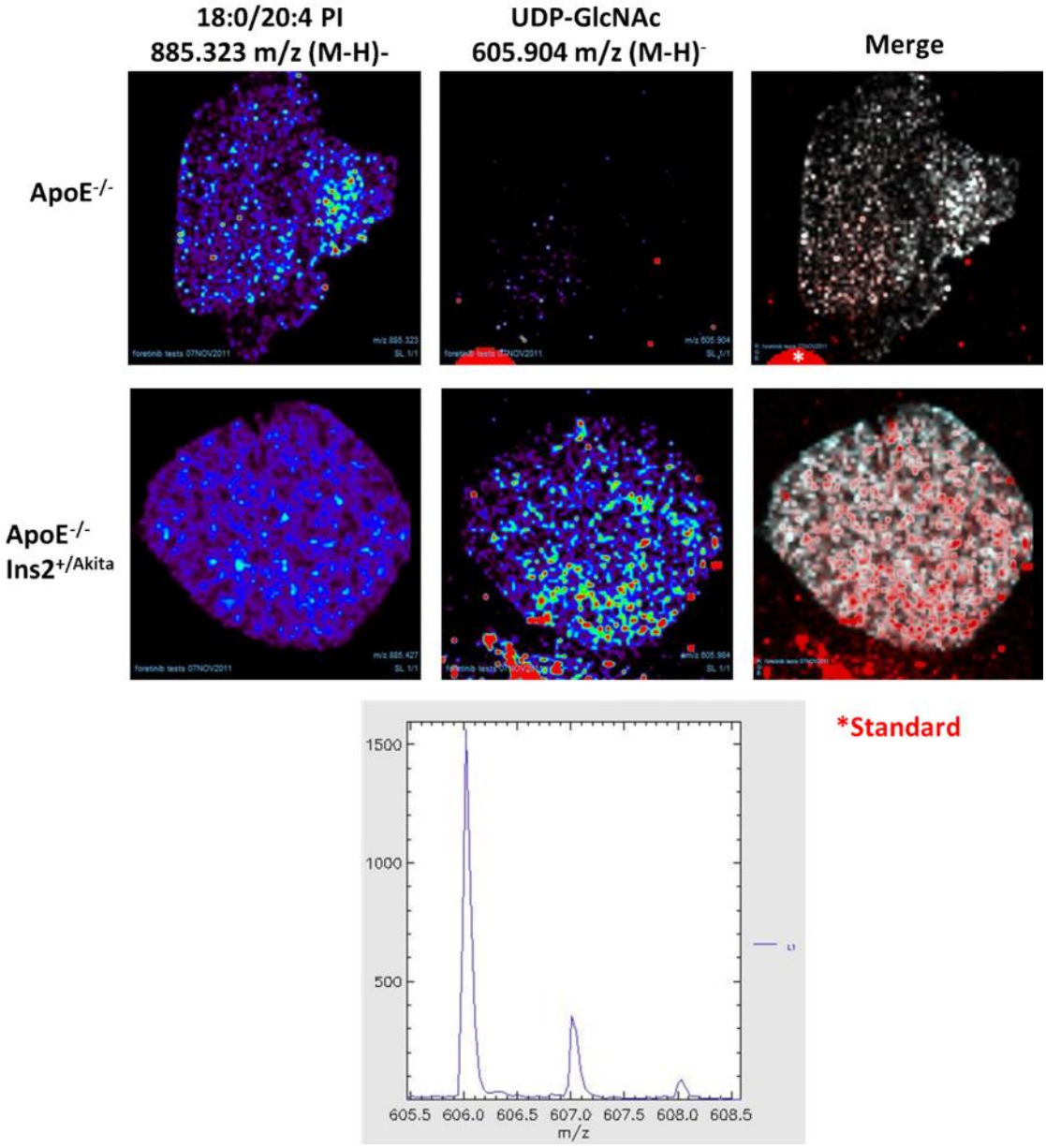

Figure 20 | MALDI-IMS analysis of livers. Images of male ApoE$^{-/-}$ (top) and Akita (bottom) liver sections showing distribution of UDP-GlcNAc (middle). PI: phosphatidylinositol is used as a control to show the structure of the tissue. A pure standard of UDP-GlcNAc spotted onto the slide is shown as a red semicircle with a white asterisk, and its mass spectrum is given. Images obtained at the Analytical Facility for Bioactive Molecules in the SickKids Research Institute in Toronto, ON.

4.4.3 Effects of hyperglycemia in skeletal muscle

As another means of investigating the role(s) of the HBP *in vivo,* immunofluorescence studies were performed to compare the expression levels of proteins associated with the HBP and ER stress in ApoE$^{-/-}$ and ApoE$^{-/-}$:Ins2$^{+/Akita}$ mice. In skeletal muscle, levels of GFAT and ER stress proteins containing the KDEL sequence were not significantly different between the normoglycemic and hyperglycemic mice (**Figure 21**). Another method used to explore the effects of hyperglycemia on the HBP was by MALDI-imaging mass spectrometry. Using this method, the distribution and abundance of UDP-GlcNAc was observed in male ApoE$^{-/-}$ and ApoE$^{-/-}$:Ins2$^{+/Akita}$ mice. The levels of this metabolite appear to be similar in the two mice (**Figure 22**).

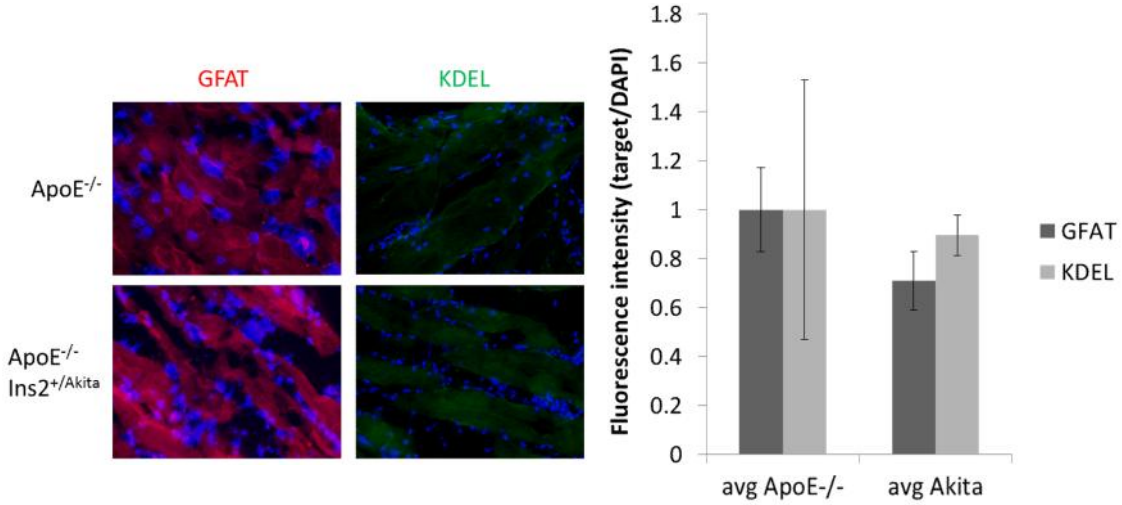

Figure 21 | Immunofluorescence analysis of skeletal muscle tissue. IF images and quantification of skeletal muscle sections from male ApoE$^{-/-}$ and ApoE$^{-/-}$Ins2$^{+/Akita}$ mice showing GFAT in red and proteins containing the KDEL sequence in green (blue=DAPI), n=4.

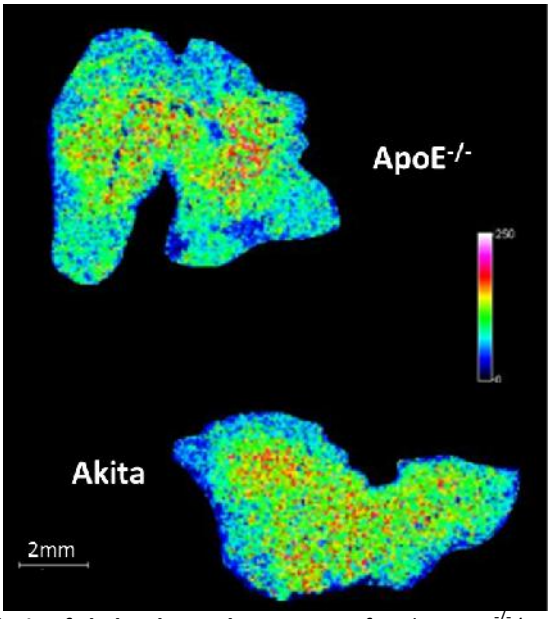

Figure 22 | MALDI-IMS analysis of skeletal muscle. Images of male ApoE$^{-/-}$ (top) and Akita (bottom) skeletal muscle sections showing the distribution and abundance of UDP-GlcNAc (m/z 606.08 ± 0.05%).

4.4.4 Effects of hyperglycemia in the aorta

Neither of the markers of HBP flux (GFAT and O-GlcNAc modified proteins) nor the ER stress proteins containing the KDEL sequence appear to be elevated in aortas of Akita mice relative to ApoE$^{-/-}$ mice (**Figure 23**). These results are consistent with those seen by MALDI-IMS, in which no difference was observed in UDP-GlcNAc levels between the two mice (**Figure 24**). However, the H&E stains revealed the presence of lesions in all of the Akita mice but only in one ApoE$^{-/-}$ mouse, suggesting that hyperglycemia accelerates the development of atherosclerosis in the Akita mice but that the site of impact may be distal, such as in the liver, rather than local (**Figure 25**). Combining these three techniques allows for a more comprehensive analysis of the role of the hexosamine

biosynthetic pathway and the factors contributing to disease progression to be performed (**Figure 26**).

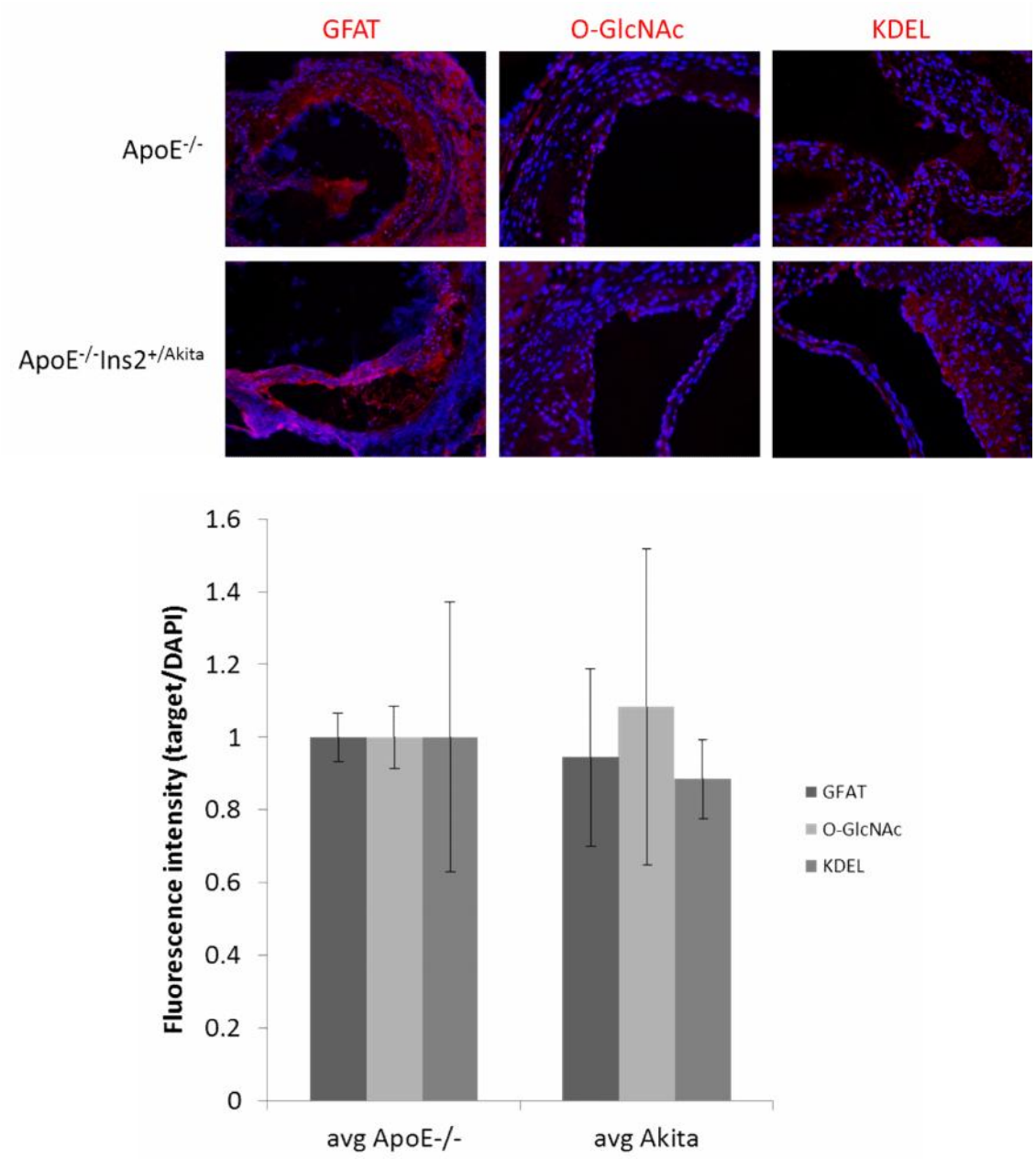

Figure 23 | Immunofluorescence analysis of aortic root sections. IF images of aortic root sections from male ApoE$^{-/-}$ and ApoE$^{-/-}$:Ins2$^{+/Akita}$ mice showing GFAT, O-GlcNAc modified proteins or proteins containing the KDEL sequence in red (blue=DAPI), n=2. The normalized fluorescence intensity is quantified below.

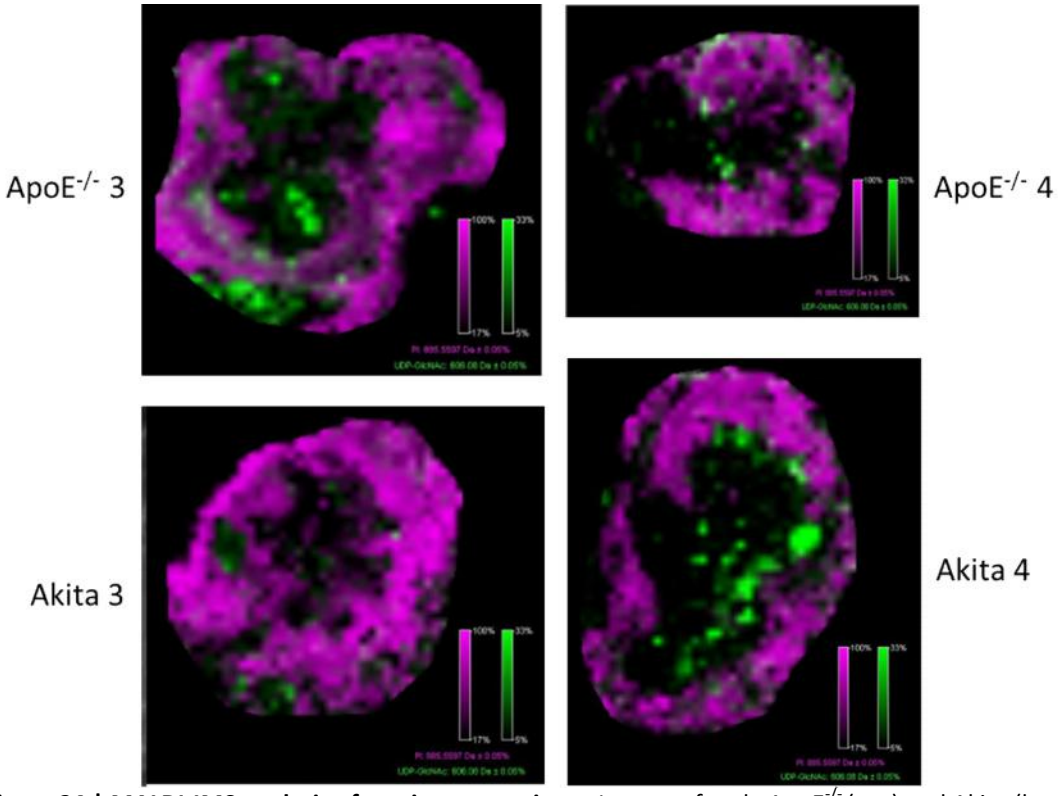

Figure 24 | MALDI-IMS analysis of aortic root sections. Images of male ApoE$^{-/-}$ (top) and Akita (bottom) aortic root sections showing the distribution of UDP-GlcNAc in green (606.08 m/z ± 0.05%) and the internal standard phosphatidylinositol in purple (885.56 m/z ± 0.05%).

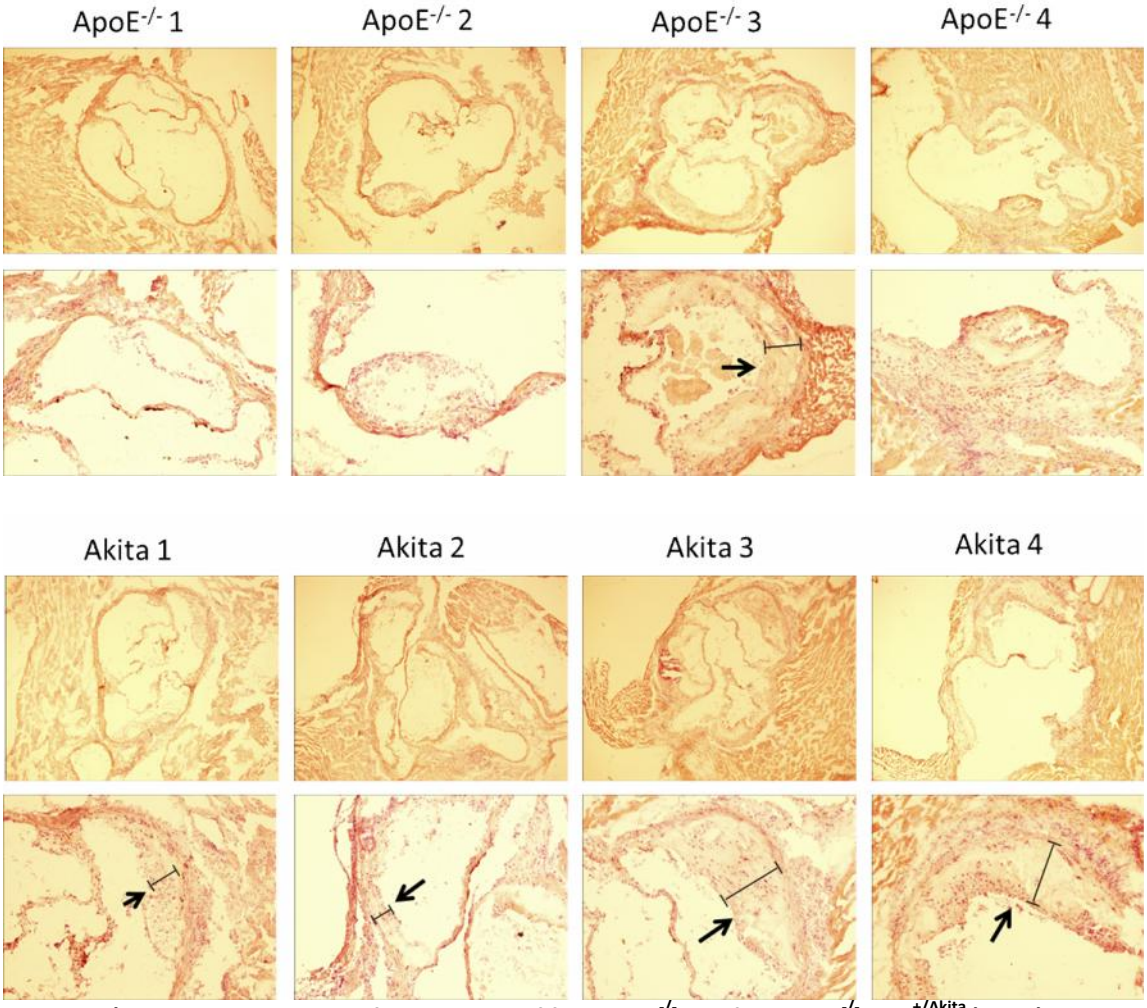

Figure 25 | Histological analysis of aortic roots of four ApoE$^{-/-}$ and four ApoE$^{-/-}$:Ins2$^{+/Akita}$ (Akita) mice. Lesions are indicated by the arrow.

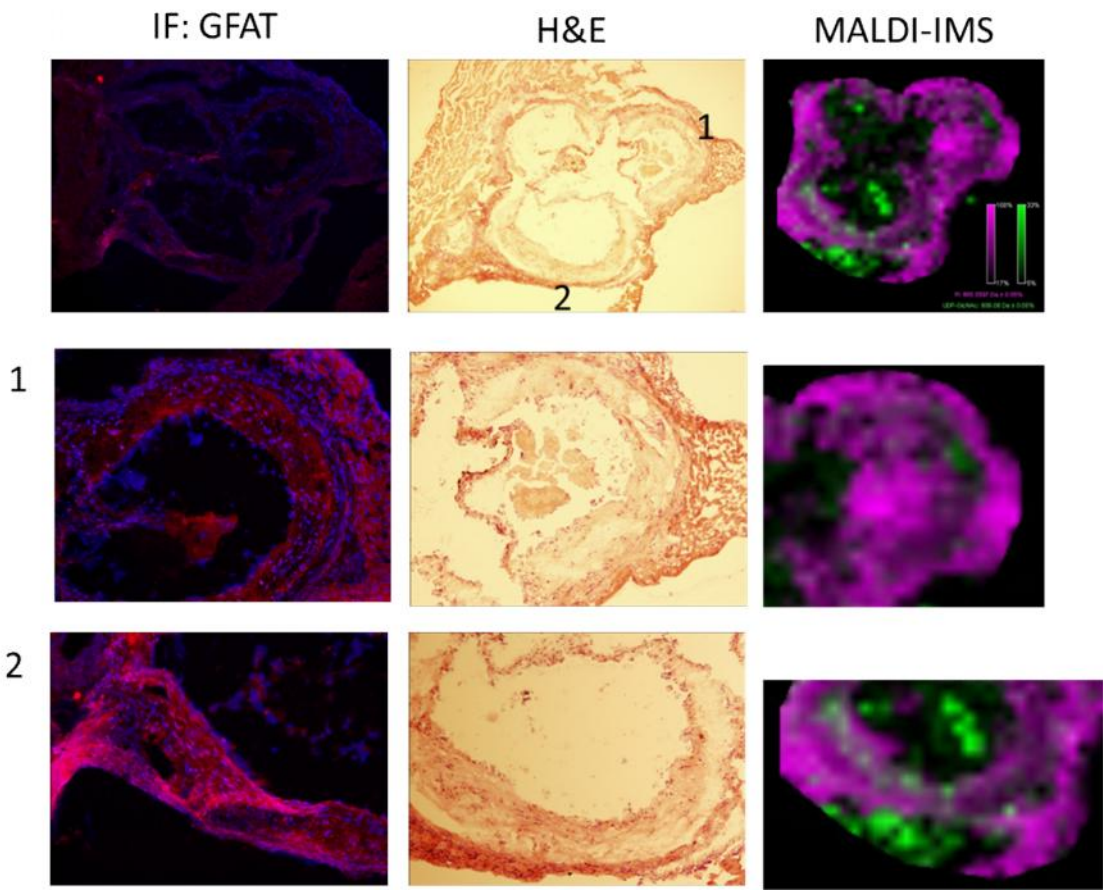

Figure 26 | Using complementary analysis techniques to study the HBP. Immunofluorescence stains (GFAT shown in red), H&E stains and MALDI-IMS images of aortic root sections from an $ApoE^{-/-}$ mouse. Two regions of interest, containing lesions, have been magnified. The H&E and MALDI-IMS images were obtained from a single section and the IF stain was performed on a consecutive section.

CHAPTER 5. DISCUSSION

The ability to measure the levels of the end product of the hexosamine biosynthetic pathway allows for a direct assessment of the effect of various treatments on pathway flux. An HPLC-MS method was developed for this purpose, using a pure standard of UDP-GlcNAc to confirm the identity of the metabolite in samples. For cultured cells, a "bead-bash" approach was used in the sample preparation phase in order to lyse the cells by non-chemical means, as this latter approach could affect the structure of the metabolite of interest. A ZIC-cHILIC column was used for separating individual compounds as this column retains polar compounds, such as sugars. Ionization and detection was performed in negative mode as UDP-GlcNAc contains negatively charged phosphate groups.

The direct effect of glucosamine on UDP-GlcNAc levels has recently been examined by HPLC-MS (*77, 78*) and the utility of our HPLC-MS system was demonstrated by the increase in UDP-GlcNAc levels observed in two different cell types (HepG2 and L6 rat skeletal muscle cells) treated with glucosamine. The reason for the significantly greater effect of glucosamine on UDP-GlcNAc levels in the skeletal muscle cells compared to the liver cancer cells is unclear; however it is possible that the turnover rate of the substrate is faster in the cancer cells, as these cells divide more rapidly, preventing the accumulation of the end product. The availability of this assay system will facilitate the further investigation of HBP activities in other cell types of interest.

The ability of glucosamine to induce ER stress has also been previously reported (*35, 37*). After verifying that glucosamine causes an increase in HBP flux, its effect on ER stress was examined. An increased expression of the ER chaperone proteins Grp78 and Grp94 was seen in both dose- and time-dependent manners. Taken together, the data are consistent with our hypothesis in that glucosamine induces ER stress through increasing UDP-GlcNAc levels. We hypothesize that the accumulation of the *N*- and *O*-linked glycosylation substrate UDP-GlcNAc adversely affects protein folding in the ER, initiating ER stress. Because ER stress triggers the activation of pathways contributing to the development of atherosclerosis, this suggests that a dysregulation in the HBP can contribute to accelerated atherosclerosis.

Glucose supplementation did not produce the same result as observed with glucosamine in either cell type examined. As excess glucose is diverted into the HBP under hyperglycemic conditions, we would expect to see a rise in UDP-GlcNAc levels compared to normoglycemic controls. Because the same result was observed in cells to which insulin was added in combination with glucose (data not shown), the hypothesis that excess glucose is not being taken up by the cells can be rejected. We hypothesize that the lack of an effect on HBP flux can be potentially attributed to the ability of HepG2 cells to regulate excessive glucose levels, as cancerous cells are known to have an altered glucose metabolism (*79*). Increasing the glucose concentration further to observe an effect on HBP flux is not an option, as these cells undergo apoptosis when

treated with ≥50 mM glucose (*80*). In the case of the skeletal muscle cells, these cells are known to be sites of high glucose utilization, thus the excess glucose may be converted into other forms such as glycogen and stored for future use instead of being diverted into the HBP (*81*).

In an attempt to link the induction of ER stress to increased flux through the HBP and to assess the ability of GFAT inhibitors to prevent the induction of ER stress, a model system in which GFAT was overexpressed using an adenovirus was employed. The adenovirus used contains a cytomegalovirus (CMV) promoter followed by a region coding for GFP, an internal ribosome entry site which allows for the initiation of translation from this region, and a GFAT coding region. The purpose of GFP is to verify successful infection, as cells that take up and express the virus will fluoresce. GFAT overexpression was confirmed by immunoblotting, which revealed that cells infected with the virus showed increased GFAT levels compared to the non-infected cells. Infection efficiency was dependent on the number of virus particles added per cell, referred to as the multiplicity of infection, and on the amount of time given for the cells to express the viral genes. Using the adenoviral system, the effect of GFAT overexpression on UDP-GlcNAc levels in HepG2 cells was examined. The results show that cells overexpressing GFAT contained higher levels of UDP-GlcNAc relative to cells infected with a control adenovirus, and these levels were similar to those seen when cells were treated with 5 mM glucosamine. Our lab has previously shown that

overexpression of GFAT induces ER stress (*35*), thus the data implies that UDP-GlcNAc levels can be lowered and the onset of ER stress can be prevented by inhibiting GFAT.

Three of the novel GFAT inhibitors identified *in vitro* by the Capretta/Werstuck groups (*51*) – amrinone (IC_{50}: 22.5 ± 2.5 μM), lapachol (IC_{50}: 4.4 ± 0.5 μM) and alloxan (IC_{50}: 4.4 ± 0.4 μM) – were further characterized in cell culture by HPLC-MS. Interestingly, alloxan has been used to chemically induce diabetes in animal models, as it generates reactive oxygen species resulting in the death of pancreatic beta cells (*69*). This paradox can be explained by the ability of glucose to protect cells against alloxan toxicity, as all cells were cultured in high glucose medium for the experiments. Alloxan is a known glucokinase inhibitor, which is the enzyme responsible for sensing glucose in beta cells, thereby preventing the glucose-induced secretion of insulin. Its mode of inhibition is based on its interaction with the thiol groups in the enzyme and glucose prevents this inhibition from occurring by binding to this site and preventing the oxidation of these thiol groups (*82*). Because of its ability to induce diabetes, alloxan itself is clearly not a suitable compound for use as a GFAT inhibitor in animal models. However, with some modifications to decrease its oxidative capacity, the core of this compound may serve as a potent non-toxic GFAT inhibitor.

All three compounds tested were able to attenuate flux through the HBP as seen by the decrease in UDP-GlcNAc levels in cells treated with the inhibitors. The peak areas of UDP-GlcNAc were normalized to those of the dipeptide internal standard Gly-Phe

added to the samples. The purpose of the internal standard is to verify that the instrument is functioning properly as the compound should elute with the same retention time and its peak should be equivalent in size in all the samples. It can also be used to correct for any loss of analyte during the sample preparation process as a concurrent decrease in the abundance of the standard would occur, keeping the ratio of the two constant thereby providing validity in the analysis. The decrease in UDP-GlcNAc levels in samples treated with inhibitors implies that the compounds retain their inhibitory properties in cultured cells without affecting cell viability, as observed in the cell counting process during sample preparation. Furthermore, the data proves that the compounds are able to cross the cell membrane and reach their target, satisfying this requirement for their potential development into pharmaceutical agents. After verifying that these compounds function in a cellular setting, additional compounds of similar structures were tested for their ability to inhibit GFAT in hopes of finding a more potent inhibitor.

In the high-throughput screen previously performed by Lisa A. Walter (*51*), several compounds containing the naphthoquinone core showed inhibitory activity towards GFAT. However, these compounds exhibit high toxicity in cultured cells when present at doses near or below their IC_{50} values. Therefore, four additional compounds with the naphthoquinone core were examined in an attempt to identify a lead compound for further development into a possible therapeutic agent. Out of the four selected, one

compound (dehydroiso-β-lapachone) abolished GFAT activity when initially tested at 5 μM. Dehydroiso-β-lapachone has an LD_{50}:IC_{50} ratio of 38:1, indicating that it does not harm cells when administered at its therapeutic dose and is therefore a good starting point for development into a more potent molecule provided the modifications made to it do not adversely affect its toxicological properties. The ability of this compound to attenuate ER stress was examined in HepG2 cells and the results show significantly decreased Grp78 and Grp94 levels in cells infected with Ad-GFP-GFAT and treated with the compound at 20 μM compared to untreated cells. However, these levels drop below those of uninfected cells, suggesting that the compound may be interfering with other biochemical processes such as the transcription of ER chaperone proteins. Furthermore, both the accumulation of unglycosylated proteins in the ER as well as over-glycosylation are associated with an overexpression of ER chaperones suggesting that the GFAT inhibitors must be used within a specific range of concentrations in order to achieve ER homeostasis (*83, 84*). In addition, ER stress levels in cells infected with Ad-GFP-GFAT are not much higher than in uninfected cells suggesting that GFAT is not being highly overexpressed, which creates a narrow window for assessing the effects of GFAT inhibitors on ER stress, thus our next goal was to seek an alternative means of increasing flux through the HBP and to consistently induce ER stress.

Since the majority of glucose entering the cell proceeds through glycolysis with only a portion being diverted into the HBP, we hypothesized that by inhibiting the

glycolytic enzyme phosphofructokinase, we could increase flux through the HBP and potentially trigger ER stress. Experiments involved treating HepG2, MOVAS and THP-1 cells with citrate and ATP – natural feedback inhibitors of the enzyme. The addition of these inhibitors resulted in only a slight increase (up to 2-fold) in levels O-linked glycosylated proteins in all cell types tested, suggesting that flux through the HBP was not dramatically increased. In addition, ER stress could not be consistently induced as seen by the lack of increase in protein expression of Grp78 and Grp94 with all cell types (data not shown). A possible explanation of these results is that the accumulation of citrate and ATP act as signals for the cell to cease glucose uptake and its breakdown through glycolysis thereby limiting the amount of glucose available to enter the HBP.

The most physiologically relevant data revealing the effects of hyperglycemia and glucosamine treatment on HBP stimulation come from direct tissue analysis. Three methods have been used for this purpose, including HPLC-MS, immunofluorescence staining and MALDI-imaging mass spectrometry. After validating our HPLC-MS system with cultured cells, we wanted to determine whether our method could be used to analyze the UDP-GlcNAc levels in blood and tissue samples. Human blood samples were taken from a healthy individual prior to, and after 2 and 4 hours of ingesting 75 g of glucose while fasting. The results did not show evidence of increased UDP-GlcNAc levels, and only a slight increase in the blood glucose concentration (from 4.5-5.6 mM after 4 hours) suggesting that a healthy human body is able to effectively deal with high levels

of glucose thereby maintaining homeostasis. This data is also consistent with results previously obtained in our lab showing that two weeks of daily glucosamine supplementation (1500 mg/day) had no effect on UPR activation. Together these results suggest that healthy human bodies can effectively deal with either a glucose or glucosamine challenge without significantly augmenting the HBP or causing ER stress. In analyzing liver samples by HPLC-MS, the addition of 5% glucosamine to the drinking water caused a 1.5-fold increase in UDP-GlcNAc levels compared to age and sex-matched control mice. This observation may have to do with the fact that the dosage of glucosamine given to these mice is 40-fold higher than that given to humans thus they are not able to regulate the levels as effectively, resulting in persistently increased HBP flux. However, the sample preparation of the tissue samples still requires optimization as large differences in metabolite levels were observed within each group of mice. This may be the reason for the lack of an observed effect of hyperglycemia on HBP flux in the livers, as the results obtained by immunofluorescence staining and MALDI-IMS show that the Akita mutation causes HBP augmentation in the liver.

Immunofluorescence staining was performed on liver tissues obtained from male $ApoE^{-/-}$ and $ApoE^{-/-}$:$Ins2^{+/Akita}$ mice. We hypothesized that the HBP would be augmented in Akita mice due to their hyperglycemic state relative to $ApoE^{-/-}$ mice. To test this hypothesis, we used immunofluorescence to probe for GFAT and O-GlcNAc-linked proteins in livers of both mice. The results showed significantly greater levels of both

GFAT and glycosylated proteins in Akita mice, implying that HBP flux is increased in these mice. These results correlate well with images of liver sections obtained by MALDI-IMS showing a significantly greater amount of UDP-GlcNAc in an Akita mouse compared to an $ApoE^{-/-}$ control. The levels of the ER chaperone proteins Grp78 and Grp94 were not different between the $ApoE^{-/-}$ and Akita mice, suggesting that hyperglycemia did not cause UPR activation in the livers of these mice. A possible explanation of this result is that the mice used to determine KDEL levels were 20 weeks of age, whereas the mice used in the GFAT and O-GlcNAc stains as well as for MALDI imaging were old breeders, thus perhaps the 20 week old hyperglycemic mice did not have an augmented HBP yet and as a result were not under ER stress.

The next tissue examined was skeletal muscle, as the HBP is known to be highly active in this tissue. Immunofluorescence staining for GFAT and ER stress proteins showed no differences in levels between the normoglycemic and hyperglycemic mice. These results correlated to those seen by MALDI imaging, where UDP-GlcNAc levels were also unchanged. These results suggest that the effects of hyperglycemia on atherosclerosis do not occur in skeletal muscle, likely because this tissue is the main site of glucose storage thus instead of constantly pushing glucose through the HBP, excess glucose may be stored at glycogen for future use.

The third region examined is at the aortic root, which is the region most relevant to atherosclerosis. No differences were seen in immunostaining for markers of HBP flux

and ER stress proteins or in UDP-GlcNAc levels through MALDI imaging between the Akita and control mice. However, the H&E stains revealed the presence of lesions in all of the Akita mice but in only one of the $ApoE^{-/-}$ mice, which is consistent with evidence from our lab showing that Akita mice have increased lesion sizes (Venegas-Pino *et al.* unpublished data) – a marker of atherosclerosis. Taken together, these data suggest that hyperglycemia promotes the accelerated development of atherosclerosis by increasing HBP flux in the liver.

The liver is the primary metabolic site for the metabolism and trafficking of lipids and ER stress has been shown to dysregulate hepatic lipid metabolism. Altered packaging, secretion and/or trafficking of low density lipoprotein cholesterol from the liver could indirectly promote atherosclerosis. In addition, the liver plays a major role in the production and secretion of plasma lipids including inflammatory cytokines. These can activate endothelial cells involved in the atherosclerotic process. More research is required in order to fully elucidate the mechanism by which the HBP mediates its effects. Nevertheless, the foundation for investigating this mechanism further has been set, where complementary methods including immunostaining, H&E staining, HPLC-MS and MALDI-IMS are used to obtain information on various aspects associated with disease progression.

CHAPTER 6. FUTURE WORK

Having established a platform for taking a metabolic approach to examine the hexosamine biosynthetic pathway and its role in accelerating atherosclerosis, these tools can now be further used to probe this pathway. In particular, HBP flux can be compared in $ApoE^{-/-}$ and $ApoE^{-/-}Ins2^{+/Akita}$ mice of different ages (eg. 10, 25 and 35 weeks) to determine when differences between the two groups of mice arise. These results can then be correlated to markers of ER stress and atherosclerosis in various tissues to determine the timing and location of different events. The utility of the MALDI imaging technique can also be expanded to examine the ER stress and atherosclerosis markers, including different types of lipids that would provide further insight into which lipid species are elevated in response to hyperglycemia and where this dysregulation is occurring.

Another way to investigate the metabolic mechanism of hyperglycemia-induced atherosclerosis is to perform a metabolomics analysis. Metabolomics refers to the non-targeted analysis of small molecule metabolites in a biological specimen (*85*). This technique has been used for several purposes including drug discovery, disease diagnosis and biomarker discovery (*85-87*). The use of metabolomics for the discovery of biomarkers of cardiovascular disease is demonstrated in a study examining metabolites from rat serum following treatment with isoproterenol as a means of inducing MI (*88*). The serum levels of thirteen lipids were found to differ between the model and control

group, implying that impairment of lipid metabolism contributes to the development of MI and that these compounds can be used as potential markers of cardiovascular disease. In regards to the role of the HBP in accelerating atherosclerosis, the metabolic profiles of control ApoE$^{-/-}$ and ApoE$^{-/-}$ mice supplemented with 5% glucosamine can be examined to determine which metabolites are either elevated or reduced between the two groups, and the timing and location of these effects. These results can then be compared to those obtained from hyperglycemia Akita mice to determine whether similar patterns of metabolite levels are observed between glucosamine treated and hyperglycemic mice. This information would increase our understanding of the role of hyperglycemia in increasing HBP flux and promoting the development of atherosclerosis. Furthermore, the metabolic profiles of non-atherosclerotic C57BL/6 mice can be compared with those of ApoE$^{-/-}$ and ApoE$^{-/-}$Ins2$^{+/Akita}$ mice with the ultimate goal of identifying a biomarker(s) in blood that could be used in a clinical setting for assessing the progression of hyperglycemia-induced atherosclerosis.

Finally, this project can be taken further to test the abilities of the GFAT inhibitors tested in the tissue culture model, or derivatives of them, to function in a mouse model. The same experiments mentioned above could be performed on Akita mice fed GFAT inhibitors to determine whether the compounds decrease HBP flux *in vivo* and to observe their effects (if any) on atherosclerosis. The hypothesis is that these inhibitors would decrease flux through the HBP thereby attenuating ER stress and the progression

of atherosclerosis. If successful, these compounds have the potential for development into therapeutics for the treatment of diabetic atherosclerosis. Ultimately, all of these experiments will expand our knowledge on the link between hyperglycemia and increased HBP flux to atherogenic pathways.

REFERENCES

1. H. C. Gerstein, Glucose: a continuous risk factor for cardiovascular disease. *Diabetic medicine : a journal of the British Diabetic Association* **14 Suppl 3**, S25 (Aug, 1997).
2. D. Mathis, L. Vence, C. Benoist, beta-Cell death during progression to diabetes. *Nature* **414**, 792 (Dec 13, 2001).
3. H. N. Ginsberg, Insulin resistance and cardiovascular disease. *The Journal of clinical investigation* **106**, 453 (Aug, 2000).
4. S. M. Haffner, S. Lehto, T. Ronnemaa, K. Pyorala, M. Laakso, Mortality from coronary heart disease in subjects with type 2 diabetes and in nondiabetic subjects with and without prior myocardial infarction. *The New England journal of medicine* **339**, 229 (Jul 23, 1998).
5. M. G. Zeadin, C. I. Petlura, G. H. Werstuck, Molecular mechanisms linking diabetes to the accelerated development of atherosclerosis. *Canadian journal of diabetes* **37**, 345 (Oct, 2013).
6. M. I. Cybulsky *et al.*, A major role for VCAM-1, but not ICAM-1, in early atherosclerosis. *The Journal of clinical investigation* **107**, 1255 (May, 2001).
7. T. Seimon, I. Tabas, Mechanisms and consequences of macrophage apoptosis in atherosclerosis. *Journal of lipid research* **50 Suppl**, S382 (Apr, 2009).
8. N. Das Evcimen, G. L. King, The role of protein kinase C activation and the vascular complications of diabetes. *Pharmacological research : the official journal of the Italian Pharmacological Society* **55**, 498 (Jun, 2007).
9. G. Basta *et al.*, Advanced glycation end products activate endothelium through signal-transduction receptor RAGE: a mechanism for amplification of inflammatory responses. *Circulation* **105**, 816 (Feb 19, 2002).
10. M. Brownlee, Biochemistry and molecular cell biology of diabetic complications. *Nature* **414**, 813 (Dec 13, 2001).
11. R. Madonna, R. De Caterina, Cellular and molecular mechanisms of vascular injury in diabetes--part I: pathways of vascular disease in diabetes. *Vascular pharmacology* **54**, 68 (Mar-Jun, 2011).
12. S. F. Yan, R. Ramasamy, A. M. Schmidt, The RAGE axis: a fundamental mechanism signaling danger to the vulnerable vasculature. *Circulation research* **106**, 842 (Mar 19, 2010).
13. H. Kaneto *et al.*, Activation of the hexosamine pathway leads to deterioration of pancreatic beta-cell function through the induction of oxidative stress. *The Journal of biological chemistry* **276**, 31099 (Aug 17, 2001).
14. M. Kunisaki, S. E. Bursell, F. Umeda, H. Nawata, G. L. King, Normalization of diacylglycerol-protein kinase C activation by vitamin E in aorta of diabetic rats and cultured rat smooth muscle cells exposed to elevated glucose levels. *Diabetes* **43**, 1372 (Nov, 1994).
15. T. A. Gardiner, H. R. Anderson, A. W. Stitt, Inhibition of advanced glycation end-products protects against retinal capillary basement membrane expansion during long-term diabetes. *The Journal of pathology* **201**, 328 (Oct, 2003).

16. A. Love, M. A. Cotter, N. E. Cameron, Effects of alpha-tocopherol on nerve conduction velocity and regeneration following a freeze lesion in immature diabetic rats. *Naunyn-Schmiedeberg's archives of pharmacology* **355**, 126 (Jan, 1997).
17. C. H. Hennekens *et al.*, Lack of effect of long-term supplementation with beta carotene on the incidence of malignant neoplasms and cardiovascular disease. *The New England journal of medicine* **334**, 1145 (May 2, 1996).
18. J. Virtamo *et al.*, Effect of vitamin E and beta carotene on the incidence of primary nonfatal myocardial infarction and fatal coronary heart disease. *Archives of internal medicine* **158**, 668 (Mar 23, 1998).
19. S. Yusuf, G. Dagenais, J. Pogue, J. Bosch, P. Sleight, Vitamin E supplementation and cardiovascular events in high-risk patients. The Heart Outcomes Prevention Evaluation Study Investigators. *The New England journal of medicine* **342**, 154 (Jan 20, 2000).
20. G. Heart Protection Study Collaborative, MRC/BHF Heart Protection Study of antioxidant vitamin supplementation in 20,536 high-risk individuals: a randomised placebo-controlled trial. *Lancet* **360**, 23 (Jul 6, 2002).
21. S. Stranges *et al.*, Effects of selenium supplementation on cardiovascular disease incidence and mortality: secondary analyses in a randomized clinical trial. *American journal of epidemiology* **163**, 694 (Apr 15, 2006).
22. I. M. Lee *et al.*, Vitamin E in the primary prevention of cardiovascular disease and cancer: the Women's Health Study: a randomized controlled trial. *JAMA : the journal of the American Medical Association* **294**, 56 (Jul 6, 2005).
23. G. H. Werstuck *et al.*, Glucosamine-induced endoplasmic reticulum dysfunction is associated with accelerated atherosclerosis in a hyperglycemic mouse model. *Diabetes* **55**, 93 (Jan, 2006).
24. A. J. Kim, Y. Shi, R. C. Austin, G. H. Werstuck, Valproate protects cells from ER stress-induced lipid accumulation and apoptosis by inhibiting glycogen synthase kinase-3. *Journal of cell science* **118**, 89 (Jan 1, 2005).
25. E. D. Schleicher, C. Weigert, Role of the hexosamine biosynthetic pathway in diabetic nephropathy. *Kidney international. Supplement* **77**, S13 (Sep, 2000).
26. P. G. Plagemann, J. Erbe, Transport and metabolism of glucosamine by cultured Novikoff rat hepatoma cells and effects on nucleotide pools. *Cancer research* **33**, 482 (Mar, 1973).
27. S. Marshall, V. Bacote, R. R. Traxinger, Discovery of a metabolic pathway mediating glucose-induced desensitization of the glucose transport system. Role of hexosamine biosynthesis in the induction of insulin resistance. *The Journal of biological chemistry* **266**, 4706 (Mar 15, 1991).
28. A. Usenik, M. Legisa, Evolution of allosteric citrate binding sites on 6-phosphofructo-1-kinase. *PloS one* **5**, e15447 (2010).
29. S. Pilkis, J. Schlumpf, J. Pilkis, T. H. Claus, Regulation of phosphofructokinase activity by glucagon in isolated rat hepatocytes. *Biochemical and biophysical research communications* **88**, 960 (Jun 13, 1979).
30. S. Milewski, Glucosamine-6-phosphate synthase--the multi-facets enzyme. *Biochimica et biophysica acta* **1597**, 173 (Jun 3, 2002).

31. A. M. Abdel Rahman, M. Ryczko, J. Pawling, J. W. Dennis, Probing the hexosamine biosynthetic pathway in human tumor cells by multitargeted tandem mass spectrometry. *ACS chemical biology* **8**, 2053 (Sep 20, 2013).
32. M. G. Buse, Hexosamines, insulin resistance, and the complications of diabetes: current status. *Am J Physiol-Endoc M* **290**, E1 (Jan, 2006).
33. W. A. Lubas, D. W. Frank, M. Krause, J. A. Hanover, O-Linked GlcNAc transferase is a conserved nucleocytoplasmic protein containing tetratricopeptide repeats. *The Journal of biological chemistry* **272**, 9316 (Apr 4, 1997).
34. A. Helenius, M. Aebi, Roles of N-linked glycans in the endoplasmic reticulum. *Annual review of biochemistry* **73**, 1019 (2004).
35. A. T. Sage *et al.*, Hexosamine biosynthesis pathway flux promotes endoplasmic reticulum stress, lipid accumulation, and inflammatory gene expression in hepatic cells. *American journal of physiology. Endocrinology and metabolism* **298**, E499 (Mar, 2010).
36. M. I. Khan, B. A. Pichna, Y. Shi, A. J. Bowes, G. H. Werstuck, Evidence supporting a role for endoplasmic reticulum stress in the development of atherosclerosis in a hyperglycaemic mouse model. *Antioxidants & redox signaling* **11**, 2289 (Sep, 2009).
37. D. R. Beriault, S. Sharma, Y. Y. Shi, M. I. Khan, G. H. Werstuck, Glucosamine-supplementation promotes endoplasmic reticulum stress, hepatic steatosis and accelerated atherogenesis in apoE-/- mice. *Atherosclerosis* **219**, 134 (Nov, 2011).
38. G. H. Werstuck *et al.*, Homocysteine-induced endoplasmic reticulum stress causes dysregulation of the cholesterol and triglyceride biosynthetic pathways. *The Journal of clinical investigation* **107**, 1263 (May, 2001).
39. B. Feng *et al.*, The endoplasmic reticulum is the site of cholesterol-induced cytotoxicity in macrophages. *Nature cell biology* **5**, 781 (Sep, 2003).
40. B. Kleizen, I. Braakman, Protein folding and quality control in the endoplasmic reticulum. *Current opinion in cell biology* **16**, 343 (Aug, 2004).
41. G. D. Holt, G. W. Hart, The subcellular distribution of terminal N-acetylglucosamine moieties. Localization of a novel protein-saccharide linkage, O-linked GlcNAc. *The Journal of biological chemistry* **261**, 8049 (Jun 15, 1986).
42. A. Helenius, How N-linked oligosaccharides affect glycoprotein folding in the endoplasmic reticulum. *Molecular biology of the cell* **5**, 253 (Mar, 1994).
43. L. A. Robertson, A. J. Kim, G. H. Werstuck, Mechanisms linking diabetes mellitus to the development of atherosclerosis: a role for endoplasmic reticulum stress and glycogen synthase kinase-3. *Canadian journal of physiology and pharmacology* **84**, 39 (Jan, 2006).
44. H. R. Pelham, The retention signal for soluble proteins of the endoplasmic reticulum. *Trends in biochemical sciences* **15**, 483 (Dec, 1990).
45. E. S. Fricovsky *et al.*, Excess protein O-GlcNAcylation and the progression of diabetic cardiomyopathy. *American journal of physiology. Regulatory, integrative and comparative physiology* **303**, R689 (Oct 1, 2012).
46. Y. Nakaishi *et al.*, Structural analysis of human glutamine:fructose-6-phosphate amidotransferase, a key regulator in type 2 diabetes. *FEBS letters* **583**, 163 (Jan 5, 2009).
47. K. O. Broschat *et al.*, Kinetic characterization of human glutamine-fructose-6-phosphate amidotransferase I: potent feedback inhibition by glucosamine 6-phosphate. *The Journal of biological chemistry* **277**, 14764 (Apr 26, 2002).

48. P. Durand, B. Golinelli-Pimpaneau, S. Mouilleron, B. Badet, M. A. Badet-Denisot, Highlights of glucosamine-6P synthase catalysis. *Archives of biochemistry and biophysics* **474**, 302 (Jun 15, 2008).
49. C. Leriche, M. A. Badet-Denisot, B. Badet, Affinity labeling of Escherichia coli glucosamine-6-phosphate synthase with a fructose 6-phosphate analog--evidence for proximity between the N-terminal cysteine and the fructose-6-phosphate-binding site. *European journal of biochemistry / FEBS* **245**, 418 (Apr 15, 1997).
50. A. G. Rajapakse, X. F. Ming, J. M. Carvas, Z. Yang, The hexosamine biosynthesis inhibitor azaserine prevents endothelial inflammation and dysfunction under hyperglycemic condition through antioxidant effects. *American journal of physiology. Heart and circulatory physiology* **296**, H815 (Mar, 2009).
51. L. A. Walter, A High-Throughput Screening Campaign To Discover Novel Inhibitors Of Human L-glutamine: D-fructose-6-phosphate Amidotransferase 1. *Open Access Dissertations and Theses* **Paper 8295.**, (2013).
52. W. T. Morgan, L. A. Elson, A colorimetric method for the determination of N-acetylglucosamine and N-acetylchrondrosamine. *The Biochemical journal* **28**, 988 (1934).
53. F. Gaucher-Wieczorek *et al.*, Evaluation of synthase and hemisynthase activities of glucosamine-6-phosphate synthase by matrix-assisted laser desorption/ionization time-of-flight mass spectrometry. *Analytical biochemistry* **458**, 61 (Aug 1, 2014).
54. J. J. Pitt, Principles and applications of liquid chromatography-mass spectrometry in clinical biochemistry. *The Clinical biochemist. Reviews / Australian Association of Clinical Biochemists* **30**, 19 (Feb, 2009).
55. J. Folch, M. Lees, G. H. Sloane Stanley, A simple method for the isolation and purification of total lipides from animal tissues. *The Journal of biological chemistry* **226**, 497 (May, 1957).
56. B. Buszewski, S. Noga, Hydrophilic interaction liquid chromatography (HILIC)-a powerful separation technique. *Anal Bioanal Chem* **402**, 231 (Jan, 2012).
57. M. Wuhrer, A. R. de Boer, A. M. Deelder, Structural glycomics using hydrophilic interaction chromatography (HILIC) with mass spectrometry. *Mass spectrometry reviews* **28**, 192 (Mar-Apr, 2009).
58. P. Kubica, A. Kot-Wasik, A. Wasik, J. Namiesnik, P. Landowski, Modern approach for determination of lactulose, mannitol and sucrose in human urine using HPLC-MS/MS for the studies of intestinal and upper digestive tract permeability. *J Chromatogr B* **907**, 34 (Oct 15, 2012).
59. T. Ikegami, K. Tomomatsu, H. Takubo, K. Horie, N. Tanaka, Separation efficiencies in hydrophilic interaction chromatography. *Journal of chromatography. A* **1184**, 474 (Mar 14, 2008).
60. F. R. A. Rouessac. (John Wiley & Sons, Ltd, Chichester, West Sussex, 2007).
61. M. Holcapek, L. Kolarova, M. Nobilis, High-performance liquid chromatography-tandem mass spectrometry in the identification and determination of phase I and phase II drug metabolites. *Analytical and bioanalytical chemistry* **391**, 59 (May, 2008).
62. M. P. Gillmeister *et al.*, An HPLC-MALDI MS method for N-glycan analyses using smaller size samples: application to monitor glycan modulation by medium conditions. *Glycoconjugate journal* **26**, 1135 (Dec, 2009).

63. R. Knochenmuss, Ion formation mechanisms in UV-MALDI. *The Analyst* **131**, 966 (Sep, 2006).
64. L. A. McDonnell, R. M. Heeren, Imaging mass spectrometry. *Mass spectrometry reviews* **26**, 606 (Jul-Aug, 2007).
65. N. Zaima *et al.*, Imaging mass spectrometry-based histopathologic examination of atherosclerotic lesions. *Atherosclerosis* **217**, 427 (Aug, 2011).
66. F. Benabdellah, D. Touboul, A. Brunelle, O. Laprevote, In situ primary metabolites localization on a rat brain section by chemical mass spectrometry imaging. *Analytical chemistry* **81**, 5557 (Jul 1, 2009).
67. M. Guilhaus, Principles and Instrumentation in Time-of-flight Mass Spectrometry. *Journal of Mass Spectrometry* **30**, 1519 (1995).
68. E. P. Rhee, R. E. Gerszten, Metabolomics and cardiovascular biomarker discovery. *Clinical chemistry* **58**, 139 (Jan, 2012).
69. S. Lenzen, The mechanisms of alloxan- and streptozotocin-induced diabetes. *Diabetologia* **51**, 216 (Feb, 2008).
70. M. Wei *et al.*, The streptozotocin-diabetic rat as a model of the chronic complications of human diabetes. *Heart, lung & circulation* **12**, 44 (2003).
71. M. L. Graham, J. L. Janecek, J. A. Kittredge, B. J. Hering, H. J. Schuurman, The streptozotocin-induced diabetic nude mouse model: differences between animals from different sources. *Comparative medicine* **61**, 356 (Aug, 2011).
72. A. J. Barber *et al.*, The Ins2Akita mouse as a model of early retinal complications in diabetes. *Invest Ophthalmol Vis Sci* **46**, 2210 (Jun, 2005).
73. J. L. Breslow, Mouse models of atherosclerosis. *Science* **272**, 685 (May 3, 1996).
74. R. L. Reddick, S. H. Zhang, N. Maeda, Atherosclerosis in mice lacking apo E. Evaluation of lesional development and progression. *Arteriosclerosis and thrombosis : a journal of vascular biology / American Heart Association* **14**, 141 (Jan, 1994).
75. K. A. Berry *et al.*, MALDI imaging MS of phospholipids in the mouse lung. *Journal of lipid research* **52**, 1551 (Aug, 2011).
76. K. R. Chalcraft, B. E. McCarry, Tandem LC columns for the simultaneous retention of polar and nonpolar molecules in comprehensive metabolomics analysis. *Journal of separation science* **36**, 3478 (Nov, 2013).
77. K. M. Hirahatake, J. K. Meissen, O. Fiehn, S. H. Adams, Comparative effects of fructose and glucose on lipogenic gene expression and intermediary metabolism in HepG2 liver cells. *PloS one* **6**, e26583 (2011).
78. K. Rilla *et al.*, Hyaluronan synthase 1 (HAS1) requires higher cellular UDP-GlcNAc concentration than HAS2 and HAS3. *The Journal of biological chemistry* **288**, 5973 (Feb 22, 2013).
79. R. J. Shaw, Glucose metabolism and cancer. *Current opinion in cell biology* **18**, 598 (Dec, 2006).
80. K. Chandrasekaran, K. Swaminathan, S. Chatterjee, A. Dey, Apoptosis in HepG2 cells exposed to high glucose. *Toxicology in vitro : an international journal published in association with BIBRA* **24**, 387 (Mar, 2010).
81. M. A. Abdul-Ghani, R. A. DeFronzo, Pathogenesis of insulin resistance in skeletal muscle. *Journal of biomedicine & biotechnology* **2010**, 476279 (2010).

82. S. Lenzen, S. Freytag, U. Panten, Inhibition of glucokinase by alloxan through interaction with SH groups in the sugar-binding site of the enzyme. *Molecular pharmacology* **34**, 395 (Sep, 1988).
83. S. C. Chang *et al.*, Rat gene encoding the 78-kDa glucose-regulated protein GRP78: its regulatory sequences and the effect of protein glycosylation on its expression. *Proceedings of the National Academy of Sciences of the United States of America* **84**, 680 (Feb, 1987).
84. V. Srinivasan, U. Tatu, V. Mohan, M. Balasubramanyam, Molecular convergence of hexosamine biosynthetic pathway and ER stress leading to insulin resistance in L6 skeletal muscle cells. *Molecular and cellular biochemistry* **328**, 217 (Aug, 2009).
85. G. A. Gowda *et al.*, Metabolomics-based methods for early disease diagnostics. *Expert review of molecular diagnostics* **8**, 617 (Sep, 2008).
86. J. Chen *et al.*, Metabonomics study of liver cancer based on ultra performance liquid chromatography coupled to mass spectrometry with HILIC and RPLC separations. *Analytica chimica acta* **650**, 3 (Sep 14, 2009).
87. J. C. Lindon, E. Holmes, M. E. Bollard, E. G. Stanley, J. K. Nicholson, Metabonomics technologies and their applications in physiological monitoring, drug safety assessment and disease diagnosis. *Biomarkers : biochemical indicators of exposure, response, and susceptibility to chemicals* **9**, 1 (Jan-Feb, 2004).
88. H. Y. Zhang *et al.*, Metabolomic profiling of rat serum associated with isoproterenol-induced myocardial infarction using ultra-performance liquid chromatography/time-of-flight mass spectrometry and multivariate analysis. *Talanta* **79**, 254 (Jul 15, 2009).